Annu. Rev. Biochem. 2004. 73:705–48
doi: 10.1146/annurev.biochem.72.121801.161542

MECHANICAL PROCESSES IN BIOCHEMISTRY

Carlos Bustamante,[1–3] Yann R. Chemla,[3]
Nancy R. Forde,[1] and David Izhaky[1]
[1]Howard Hughes Medical Institute and the Departments of [2]Molecular and Cell Biology, and [3]Physics, University of California, Berkeley, California 94720-3206; email: carlos@alice.berkeley.edu, ychemla@socrates.berkeley.edu, nforde@alice.berkeley.edu, izhaky@alice.berkeley.edu

Key Words mechanical forces, single-molecule manipulation, molecular motors, mechanical unfolding, enzyme catalysis

■ **Abstract** Mechanical processes are involved in nearly every facet of the cell cycle. Mechanical forces are generated in the cell during processes as diverse as chromosomal segregation, replication, transcription, translation, translocation of proteins across membranes, cell locomotion, and catalyzed protein and nucleic acid folding and unfolding, among others. Because force is a product of all these reactions, biochemists are beginning to directly apply external forces to these processes to alter the extent or even the fate of these reactions hoping to reveal their underlying molecular mechanisms. This review provides the conceptual framework to understand the role of mechanical force in biochemistry.

CONTENTS

PROLOGUE

Fifty years ago, biochemists described cells as small vessels that contain a complex mixture of chemical species undergoing reactions through diffusion and random collision. This description was satisfactory inasmuch as the intricate pathways of metabolism and, later, the basic mechanisms of gene regulation and signal transduction were still being unraveled. Gradually, and in part as a result of the parallel growth in our structural understanding of the molecular components of the cell, the limitations of this "chemical reactor" view of the cell became plain. Armed with a more precise knowledge of the structural bases of molecular interactions, the focus shifted more and more to the mechanisms by which these molecular components recognize and react with each other. Moreover, it also became clear that cells are polar structures and that the cell interior is neither isotropic nor homogeneous; that many of the essential processes of the cell, such as chromosomal segregation, translocation of organelles from one part of the cell to another, protein import into organelles, or the maintenance of a voltage across the membrane, all involve directional movement and transport of chemical species, in some cases against electrochemical gradients. Processes such as replication, transcription, and translation require directional readout of the information encoded in the sequence of linear polymers. Slowly, the old paradigm was replaced by one of a small "factory" of complex molecular structures that behave in machine-like fashion to carry out highly specialized and coordinated processes. These molecular machines are often complex assemblies of many proteins and contain parts with specialized functions, for example, as energy transducers or molecular motors, converting chemical energy (either in the form of binding energy, chemical bond hydrolysis, or electrochemical gradients) into mechanical work through conformational changes and displacements.

To understand the behavior of this molecular machinery requires a fundamental change in our conceptual and practical approaches to biochemical research. The cell, it appears, resembles more a small clockwork device than a reaction vessel of soluble components. Many of the functions of this device (which besides replication, transcription, translation, and organelle transport, include cell crawling, cell adhesion, protein folding, protein and nucleic acid unfolding, protein degradation, and protein and nucleic acid splicing) are indeed mechanical processes, and basic physical concepts such as force, torque, work, energy conversion efficiency, mechanical advantage, etc., are needed to describe them. The recent development of experimental methods that permit the direct

mechanical manipulation of single molecules now allows many of these mechanical processes to be investigated directly and in real-time fashion. Analyses of the data so obtained also require the reformulation of many of the traditional concepts of thermodynamics and kinetics to incorporate terms corresponding to forces and torques.

This article attempts to critically review the most recent conceptual and experimental developments in the mechanical characterization of biochemical processes. In the following section we reformulate some of the main results of thermodynamics and kinetics in terms of the effect of mechanical force to provide a conceptual framework for the interpretation of the results presented later in this review. In the third section, we review the use of mechanical force to unfold proteins and nucleic acids. Here, as in the following sections, we describe and illustrate the important new information that can be derived from the mechanical characterization of molecules and molecular processes rather than providing an exhaustive guide to the literature. In the fourth section we describe the mechanical properties of molecular motors, illustrate how mechanical force is used to investigate their mechanisms of mechanochemical transduction, and discuss the many cellular functions now known to be mechanical processes. The final section presents our current understanding of the importance of force and strain in enzyme catalysis: how an otherwise silent form of chemical energy (that associated with binding interactions) can be and is used by enzymes to accelerate the rate of chemical reactions in the cell.

The mechanical characterization of the cellular "factory" is just beginning. Many more mechanical cellular functions are likely to be discovered in the future. This exciting new aspect of the inner workings of the cell challenges us to learn to think in terms of concepts heretofore alien to the trained biochemist. We hope that this review will be a helping step in that direction.

THE EFFECT OF FORCE ON THE THERMODYNAMICS AND KINETICS OF CHEMICAL REACTIONS

Introduction

Many biochemical reactions proceed via large conformational changes within or between interacting molecules. Such conformational changes, which may involve a combination of linear and rotational degrees of freedom, provide convenient, well-defined mechanical reaction coordinates that can be used to follow the progress of the reaction. Examples of these reaction coordinates are the end-to-end distance of a molecule as it is being stretched, the position of a molecular motor as it moves along a track, the angle of a rotary motor's shaft, or the deformation of an enzyme's binding pocket when it binds the substrate. The effect of an applied force can yield valuable information about the free energy surface of the reaction. In this section, we describe, using basic thermodynamic

and kinetic relationships, how an applied mechanical force affects the free energy, equilibrium, and rate of a reaction occurring along a mechanical reaction coordinate (for a more detailed treatment, see 1). For brevity, and because of its direct relevance to the majority of the examples in this review, we limit our discussion to linear mechanical reaction coordinates. By replacing linear distance by angle and force by torque, it is possible to derive analogous expressions for the effect of torsion.

From thermodynamics, the energy change of a system (e.g., a molecule being stretched, a motor moving along a track, etc.) can be separated into components related to the heat exchanged and the work done on or performed by the system. When the energy changes slowly enough that the system remains in quasi-static equilibrium, these quantities are the reversible exchanged heat and the reversible work (pressure-volume work and mechanical work):

$$\begin{aligned} dE &= dq_{rev} + dw_{rev} \\ &= (TdS) + (-PdV + \int F \cdot dx). \end{aligned} \quad 1.$$

In practice, the temperature and pressure are usually the independent variables in an experiment, and the Gibbs free energy ($G = E - TS + PV$) provides a more relevant expression:

$$dG = -SdT + VdP + Fdx. \quad 2.$$

At constant temperature and pressure, the work required to extend the system by an amount Δx is

$$W = \int_{x_0}^{x_0 + \Delta x} Fdx. \quad 3.$$

If the extension is carried out slowly enough that the system remains in quasi-static equilibrium, the work in Equation 3 is reversible and is equal to the free energy change of the system, $\Delta G_{stretch}(\Delta x)$. The work done to stretch the molecule is positive, as both F and Δx are positive. Positive work means that the surroundings have done work on the system; the free energy of the molecule is increased.

Work is required to stretch a DNA molecule by its ends, and the amount of force required to extend its ends a given distance is described by the worm-like chain model of polymer elasticity (2, 3). When the molecule is relaxed, the tension in the DNA molecule decreases and the molecule does work on its surroundings. The molecule follows the same force-extension curve upon stretching as relaxation, implying that these processes are occurring at equilibrium. Thus, DNA acts as a reversible spring, storing elastic energy as it is stretched and restoring that same energy to the surrounding bath as it relaxes. In other words,

mechanical stretching and relaxation of DNA are 100% efficient, when all of input (or stored) work is converted to a free energy change of the molecule and none is dissipated as heat. By integrating the area under the force-extension curve of DNA, the free energy change in the molecule due to stretching [$\Delta G_{stretch}$(x)] can thus be determined (Equation 3). Furthermore, by measuring the free energy change as a function of temperature, it is possible to determine the change in entropy, $\Delta S_{stretch}$, and the change in enthalpy, $\Delta H_{stretch}$, upon stretching the molecule. Recalling that the enthalpy $H = G\text{-}TS$ and using Equation 2, it can be shown that:

$$\Delta S_{stretch}(x) = -\left(\frac{\partial \Delta G_{stretch}(x)}{\partial T}\right)_{P,x}, \quad \Delta H_{stretch}(x) = \left(\frac{\partial (\Delta G_{stretch}(x)/T)}{\partial (1/T)}\right)_{P,x}. \qquad 4.$$

Effect of Force on the Free Energy of a Reaction

The effect of force on a reaction in which A is converted into B is illustrated by the two-state system depicted in Figure 1. Here, A and B are distinct observable states of the system; each occupies a local free energy minimum, at position x_A and x_B, respectively, separated by a distance Δx along the mechanical reaction coordinate shown in Figure 1. A and B could represent the states of a motor in sequential locations along its track, or folded and unfolded states of a protein. At zero force, the free energy difference between A and B is simply

$$\Delta G(F = 0) = \Delta G^0 + k_B T \, ln \frac{[B]}{[A]}, \qquad 5.$$

where ΔG^0 is the standard state free energy, and $[A]$ and $[B]$ are the concentrations (more appropriately, the activities) of the molecule in states A and B. Since concentrations are only well-defined in bulk measurements, $[A]$ and $[B]$ represent probabilities of populating states A and B in single-molecule experiments. To a first approximation, an applied force "tilts" the free energy surface along the mechanical reaction coordinate by an amount linearly dependent on distance (Equation 2), such that

$$\Delta G(F) = \Delta G^0 - F(x_B - x_A) + k_B T \, ln \frac{[B]}{[A]}. \qquad 6.$$

At equilibrium, $\Delta G = 0$ and

$$\begin{aligned} \Delta G^0 - F\Delta x &= -k_B T \, ln \frac{[B]_{eq}(F)}{[A]_{eq}(F)} \\ &= -k_B T \, ln \, K_{eq}(F). \end{aligned} \qquad 7.$$

Thus, the equilibrium constant $K_{eq}(F)$ depends exponentially on the applied force. By applying a force assisting ($F > 0$) or opposing ($F < 0$) the transition, we can alter the equilibrium of the reaction, increasing or reducing the population

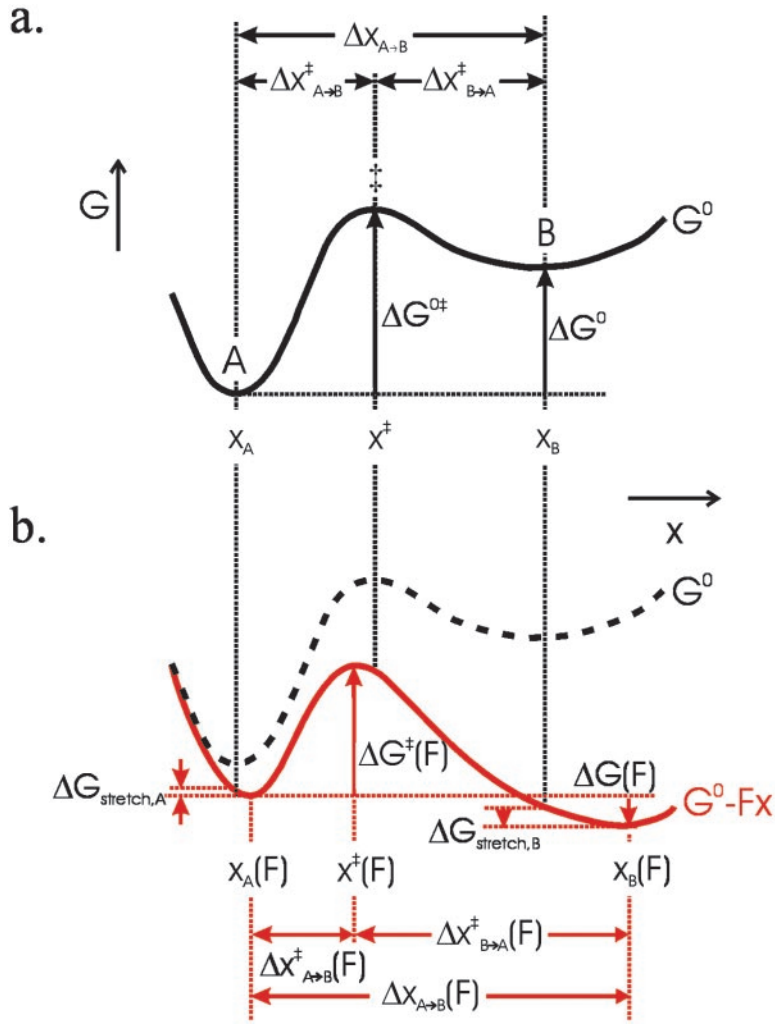

Figure 1 The effect of force on the free energy of a two-state system, where x represents the mechanical reaction coordinate. (*a)* No applied force. (*b*) Solid curve: positive applied force. Dashed curve: no applied force. The application of force lowers the energy of both the transition state ‡ and state B relative to state A ($\Delta G^{0\ddagger}$ and ΔG^0), which increases the rate of the forward reaction and the population of state B, respectively. The positions of the free energy minima (x_A and x_B) and maximum ($x^{\ddagger}$) shift to longer and shorter x, respectively, with a positive applied force. Their relative shifts in position depend on the local curvature of the free energy surface. The free energy change of states A and B upon stretching is $\Delta G_{stretch}$; see text.

of state B relative to state A, respectively. Furthermore, from Equation 7, one can determine the separation, Δx, between states A and B from the slope of the plot of $\ln K_{eq}(F)$ against the force.

For simplicity, we have assumed that the positions of states A and B, x_A and x_B, are unaffected by an applied force. In general, this assumption is not valid. As an example of the reaction A→B, consider the mechanical unfolding of a protein by its ends. As shown in Figure 1, force not only shifts the equilibrium toward state B (the unfolded state), but also increases the average end-to-end distance x_B of the unfolded molecule from that of a zero-force, random-coil configuration $x_B(F = 0)$ to that of an extended polypeptide chain $x_B(F)$. It is clear from Figure 1 that the shifts in x_A and x_B with force depend inversely on the local curvature of the potential: the steeper the potential well, the more "localized" the state, and the lesser the effect of force on its position. (For a harmonic potential well, the minimum shifts by F/G'', where G'' is the second derivative of the free energy surface at the minimum.) In Figure 1, the end-to-end distance of the folded protein (x_A) is less shifted by force than that of the unfolded molecule (x_B).

Because the free energy of the reaction A→B under an applied force F must be measured between the new free energy minima at $x_B(F)$ and $x_A(F)$, Equation 7 must be corrected to account for the small free energy change due to this shift in minima:

$$\Delta G^0 - F\Delta x + \Delta G^{A\to B}_{stretch}(F) = -k_B T \ln K_{eq}(F) \qquad 8.$$

where $\Delta x = x_B(F = 0) - x_A(F = 0)$ and $\Delta G^{A\to B}_{stretch}(F)$ is given by

$$\begin{aligned}\Delta G^{A\to B}_{stretch}(F) &= \Delta G_{stretch,B}(F) - \Delta G_{stretch,A}(F)\\ &= \int_{x_B(F=0)}^{x_B(F)} F_B dx_B - \int_{x_A(F=0)}^{x_A(F)} F_A dx_A.\end{aligned} \qquad 9.$$

The two terms in Equation 9 are the free energy differences due to the shift in the minimum at state B [i.e., the free energy of stretching the molecule from $x_B(0)$ to $x_B(F)$] and at state A [stretching from $x_A(0)$ to $x_A(F)$], respectively (see Figure 1). If states A and B have the same curvature, their minima are shifted by the same amounts. In this situation, the two terms in Equation 9 cancel out exactly, and

$$\Delta G^{A\to B}_{stretch}(F) = 0.$$

This would be the case for a molecular motor moving along a homogeneous track, where states A and B represent sequential positions on the track.

We have seen that force can shift the equilibrium of a reaction. In principle, it is possible to apply a force, $F_{1/2}$, such that the equilibrium constant $K_{eq} = 1$. At $F_{1/2}$, the molecule has an equal probability of being in state B or A, and will

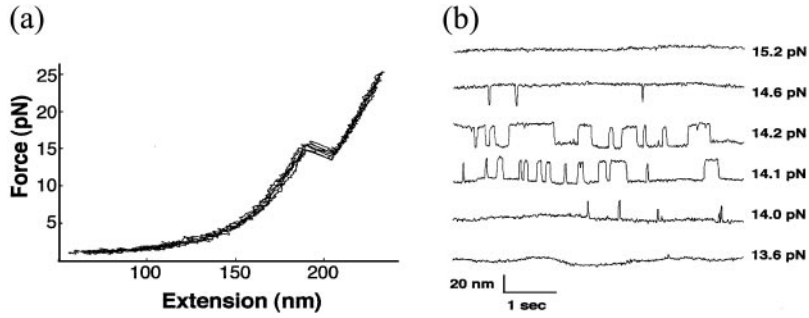

Figure 2 Mechanical unfolding of the 22-bp P5ab RNA hairpin, a domain of the group I intron of *T. thermophila* (4). (*a*) The force-extension curve shows a discontinuity at ~15 pN, due to the hairpin unfolding. The transition is occurring reversibly, as evidenced by the perfect overlap between the stretching and relaxing curves. (*b*) If the molecule is maintained at a constant force near the transition, it "hops" between the folded and unfolded states. Increasing the force through the transition, the hairpin ranges from being predominantly folded (13.6 pN, *bottom curve*), to being predominantly unfolded (15.2 pN, *top*). At the midway point, at a force of ~14.5 pN ($F_{1/2}$), the molecule spends half its time in the folded state and half in the unfolded state.

thus spend half its time in each state. From Equation 8, it is evident that $F_{1/2}$ provides a direct measure of the standard state free energy:

$$F_{1/2} \cdot \Delta x = \Delta G^{0} + \Delta G^{A \to B}_{stretch}(F), \qquad 10.$$

where here we include the contribution of the free energy of stretching, $\Delta G_{stretch}$. Furthermore, by taking derivatives of Equation 10 with respect to temperature and inverse temperature (as in Equation 4), one can determine the entropy and enthalpy, respectively, of the reaction:

$$\begin{aligned} \frac{\partial (F_{1/2} \cdot \Delta x)}{\partial T} &= -\Delta S^{0} - \Delta S^{A \to B}_{stretch}(F), \\ \frac{\partial (F_{1/2} \cdot \Delta x/T)}{\partial (1/T)} &= \Delta H^{0} + \Delta H^{A \to B}_{stretch}(F). \end{aligned} \qquad 11.$$

The effect of force on the free energy of a reaction is illustrated experimentally by the mechanical unfolding of a simple RNA hairpin (4, 5). The force-extension curve of the molecule (Figure 2*a*) shows a discontinuity at ~15 pN, where the length suddenly increases, due to the hairpin unfolding. Upon relaxation, the molecule follows the same force-extension curve, indicating that the unfolding process is occurring reversibly. From the area under the transition, Equation 3 can be used to calculate the free energy of unfolding the molecule mechanically, $\Delta G^{0} + \Delta G_{stretch}$. By correcting this value for $\Delta G_{stretch}$, the standard free energy

of unfolding was determined, giving $\Delta G^0 = 113 \pm 30$ kJ/mol, a value that agrees well with the predicted free energy value of 147 kJ/mol for unfolding in solution (4).

Effect of Force on the Kinetics of a Reaction

The effect of a mechanical force on the kinetics of a reaction was first described by Bell in 1978, in the context of cellular adhesion (6). Here we apply the concept of a tilted free energy surface to describe the force dependence of kinetic rates. For reactions occurring in solution where inertial forces are negligible, the theory of Kramers (7) gives the rates of transitions between states A and B as

$$k_{A\to B} = \frac{\omega_A \omega^{\ddagger}}{2\pi\gamma/m} e^{-\Delta G^{0\ddagger}/k_B T}, \quad k_{B\to A} = \frac{\omega_B \omega^{\ddagger}}{2\pi\gamma/m} e^{-(\Delta G^0 + \Delta G^{0\ddagger})/k_B T}. \qquad 12.$$

The rates depend exponentially on the activation free energies (differences between free energies of the transition state ‡ and states A and B, for the forward and reverse reactions, respectively). The pre-exponential factors in Equation 12 are related to the rates at which the molecule diffuses[1] to the transition state from states A and B, respectively; they depend on the characteristic frequency ω_A (ω_B) of the harmonic potential well at state A (B), which sets the rate at which the molecule "attempts" to overcome the barrier, $\omega^{\ddagger}$, which sets the rate of passage over the transition state once it has been reached, and the ratio of the friction coefficient experienced by the molecule to its mass, γ/m, which is the damping rate. The characteristic frequencies depend on the curvature of the free energy surface at each state ($\omega_A{}^2 = G''(x_A)/m$, etc.). Because force "tilts" the free energy along the mechanical reaction coordinate, if an external force assists the forward transition A→B, then the transition state free energy relative to that of state A is lowered by an amount $F\Delta x^{\ddagger}_{A\to B}$, where $\Delta x^{\ddagger}_{A\to B} = x^{\ddagger} - x_A$ (see Figure 1). Conversely, the free energy difference between state B and the transition state ‡ is increased by $F\Delta x^{\ddagger}_{B\to A} = F(\Delta x_{A\to B} - \Delta x^{\ddagger}_{A\to B}) = F(x_B - x^{\ddagger})$. As a result, the forward and reverse rates are modified exponentially by the external force:

$$k_{A\to B}(F) \sim e^{-\left(\Delta G^{0\ddagger} - F\Delta x^{\ddagger}\right)/k_B T}, \quad k_{B\to A}(F) \sim e^{-\left(\Delta G^{0\ddagger} - \Delta G^0 + F\left(\Delta x - \Delta x^{\ddagger}\right)\right)/k_B T} \qquad 13.$$

Here, we have again assumed that the locations of A, B, and the transition state are force independent, which as discussed above is not true in general. Positive force shifts the positions of minima to longer extensions, while the positions of

[1]Global protein displacements, such as the movement of a molecular motor along its track (discussed below), are expected to occur in the overdamped limit and are well described by diffusion. In cases where conformational changes are underdamped, the prefactors in Equation 12 are modified and do not depend on the damping rate (7). In the Eyring model (8), applicable when covalent bonds are made or broken, the prefactor corresponds to a single quantum mechanical vibrational frequency of the molecule. In all of these models, however, the exponential dependence of the transition rate on the barrier free energy is maintained.

maxima are shifted to shorter extensions. Thus, the distance changes, $\Delta x^{\ddagger}_{A\to B}$ and $\Delta x^{\ddagger}_{B\to A}$, that affect the rates are altered with applied force, no matter what the local curvature of the free energy surface. When states A, B, and ‡ have steep curvature, these shifts are negligible. For molecular unfolding, this is not the case, as is discussed in the following section.

Returning to our example of the RNA hairpin, we illustrate what can be learned by studying the force-dependent kinetics of the folding-unfolding reaction. Remarkably, by holding the force constant at a value near 15 pN, the hairpin is seen to "hop" between its folded and unfolded states (Figure 2*b*). Thus, this experiment makes it possible to follow the reversible unfolding of a single molecule in real time. No intermediates are observed and the reaction can be treated as a cooperative, two-state process. The distributions of dwell times in the folded state and in the unfolded state give the unfolding and refolding rate coefficients, respectively, whose force dependence can be determined. As shown in Equation 13, the force dependence of the rate coefficient for unfolding gives the distance from the folded to the transition state $\Delta x^{\ddagger}_{f\to u}$ along the mechanical reaction coordinate:

$$k_{f\to u}(F) = k^{0}_{f\to u}\, exp\frac{F\Delta x^{\ddagger}_{f\to u}}{k_B T}. \qquad 14.$$

where $k_{f\to u}{}^{0}$ is the unfolding rate constant along this pathway at zero force. For this molecule, the transition state is found to be midway between the folded and unfolded states ($\Delta x^{\ddagger}_{f\to u} = 11.9$ nm and $\Delta x^{\ddagger}_{u\to f} = 11.5$ nm).

The equilibrium constant for the $f \rightleftharpoons u$ reaction and its force dependence can also be determined from the ratio of dwell times of the molecule in the unfolded and folded states at any given force:

$$K_{eq}(F) = \tau_u(F)/\tau_f(F). \qquad 15.$$

As shown in Figure 2*b*, the hopping of the hairpin from the folded to the unfolded state depends on the force. By determining the probability of populating the folded and unfolded states as a function of force, the midpoint of the transition is found to occur at $F_{1/2} = 14.5$ pN. At this force, the molecule spends half its time folded and half unfolded, and $K_{eq} = 1$. From Equation 10, a value of 149 ± 16 kJ/mol is determined for the free energy of unfolding, ΔG^{0}. $K_{eq}(F)$ is found to depend exponentially on applied force, as predicted by Equation 7 (4). From the force dependence of the equilibrium constant, the distance $\Delta x_{f\to u}$ between the folded and unfolded states is calculated to be 23 ± 4 nm, which agrees well with the expected length increase upon opening a 22-bp hairpin. By extrapolating $K_{eq}(F)$ to zero force, ΔG^{0} can also be calculated. The value obtained by this method, 156 ± 8 kJ/mol, agrees well with that found from the area under the force-extension curve and from $F_{1/2}$. In general, because the kinetics of a reaction is pathway-dependent, extrapolation of kinetically determined param-

eters to zero force can give misleading results. We return to this point in the following section.

MECHANICAL UNFOLDING

Introduction

Many biological molecules have a defined mechanical function. For these molecules, their resistance to unfolding in response to an applied mechanical force—their mechanical stability—is of critical physiological importance. For example, titin is the protein responsible for passive elasticity in the skeletal and cardiac muscle sarcomere, where it functions as a molecular spring and ensures the return of the sarcomere to its initial dimensions after muscle relaxation (9–11). Fibronectin and tenascin are components of the extracellular matrix, where they extend and contract to facilitate, for example, cell migration and adhesion (12, 13). Regulation of the latter is thought to be controlled by a force-dependent recognition site in fibronectin (14). These mechanical proteins have in common a tandem arrangement of β-barrel domains, linked by segments of unstructured polypeptides. In contrast, spectrin is an α-helical protein that plays a central role in the mechanical properties of erythrocytes, which must deform and squeeze through narrow blood vessels during flow (37).

Whereas the examples above demonstrate the importance of a molecule's mechanical stability to its own function, many cellular processes involve the unfolding of macromolecules. For instance, secondary and higher-order nucleic acid structures have to be disrupted to permit translocation by RNA and DNA polymerases, the ribosome, and DNA and RNA helicases. An increasing body of evidence indicates that these machine-like molecules exert mechanical force on their substrates to perform their cellular functions. Similarly, examples of protein "unfoldases" include the import machinery of organelles (15), proteasomes (15, 16), and chaperonins (17–18), all of which use chemical energy from ATP to actively unfold (or fold) proteins. Many of these unfolding processes are likely to be mechanical in nature, although their direct characterization is only now becoming experimentally possible.

While direct measurements of forces in vivo during these types of cellular processes await future technical developments, much can be learned by studying well-defined model systems in vitro and characterizing their responses to force. The development of techniques for manipulating and exerting force on individual molecules enables us to define, for the first time, the conditions under which a molecule unfolds in response to an applied mechanical force. These early studies have revealed a broad distribution of mechanical stabilities among macromolecules, and have found that a molecule's *mechanical* stability cannot be predicted from its thermodynamic stability. Thus, mechanical stability is a property not directly accessible through bulk experiments, and must be determined by direct

mechanical measurements. Here, we discuss the mechanical unfolding of proteins and nucleic acids, and how parameters such as the magnitude, direction, and time-dependence of the applied force affect the mechanical stability of these macromolecules.

Irreversibility in Mechanical Unfolding Experiments

When the mechanical unfolding of a macromolecule occurs at equilibrium, it is possible to determine directly the free energy, equilibrium constant and kinetics of the reaction and their dependence on force. We discussed in the previous section how this information can be obtained from reversible, coincident folding and unfolding curves for the example of the mechanical unfolding of a simple RNA hairpin. When the extension and relaxation curves do not overlap, folding/unfolding transitions are not occurring reversibly. From the second law of thermodynamics, the average work done to mechanically unfold the molecule is greater than the free energy of unfolding:

$$W_{irrev} > \Delta G. \qquad 16.$$

Mechanical unfolding under these conditions is less than 100% efficient because not all of the mechanical work put in to unfold the molecule is converted to a change in the free energy of the molecule. However, for a two-state system, it has recently been demonstrated that it is possible to recover the free energy of unfolding even when the reaction is not occurring at equilibrium (19–21). This result takes advantage of the ability of single-molecule experiments to provide the distribution of unfolding forces (and hence, work done), rather than just the mean value.

More often than not in mechanical unfolding experiments, hysteresis is observed between the extension and relaxation curves, indicating that the molecule is being extended or relaxed at a rate faster than its rate of equilibration. For the molecule to equilibrate during stretching or relaxation, the total change in force applied to the molecule during its slowest relaxation time τ must be less than the root-mean-square force fluctuations it would experience at equilibrium, i.e., $r\tau \leq \Delta F_{rms}$, where the loading rate $r \equiv dF/dt$ (pN/sec) (1). This is the requirement for quasistatic equilibrium during stretching or relaxation. Although most single-molecule mechanical unfolding experiments are performed under nonequilibrium conditions, the observed unfolding force distribution can provide useful information about the free energy surface, such as the position of the transition state. The observed unfolding force distribution is peaked, and the most probable unfolding force F_u* increases with loading rate as (1)

$$F_u^* = \frac{k_B T}{\Delta x_{f\to u}^{\ddagger}} ln\left(\frac{r\Delta x_{f\to u}^{\ddagger}}{k_{f\to u}^{0} k_B T}\right). \qquad 17.$$

This maximum arises from the convolution of two competing trends: the probability that a domain remains folded decreases with time (and hence with

force, since typically $F = 1n(r)$, whereas the probability of unfolding increases with force (22). The slope of a plot of F_u* versus 1n(r) yields $\Delta x^{\ddagger}_{f\to u}$, whereas the intercept gives the unfolding rate along the mechanical reaction coordinate at zero force $k^0_{f\to u}$.

Why the unfolding force depends on loading rate can be understood by considering the rate of energy input that drives molecular unfolding. Recalling that $k^0_{f\to u} = A\exp(-\Delta G^{\ddagger}/k_BT)$ (Equation 12, where here we denote with A the exponential prefactor), we can rewrite Equation 17 as

$$F^*_u = \frac{\Delta G^{\ddagger}}{\Delta x^{\ddagger}_{f\to u}} + \frac{k_BT}{\Delta x^{\ddagger}_{f\to u}} ln\left(\frac{r\Delta x^{\ddagger}_{f\to u}}{Ak_BT}\right). \quad 18.$$

The second term vanishes whenever

$$r\Delta x^{\ddagger}_{f\to u} = Ak_BT. \quad 19.$$

The term on the left represents the rate of energy delivery into the system from the pulling process; the term on the right represents the rate of energy exchange with the surrounding thermal bath. Under balanced energy exchange conditions, where these are equal, the unfolding force is equal to the ratio of activation energy to the distance to the barrier. If $r\Delta x^{\ddagger}_{f\to u} \ll Ak_BT$, by contrast, $F_u^* < \Delta G^{\ddagger}/\Delta x^{\ddagger}_{f\to u}$ and the process is largely thermally activated. In most unfolding experiments, however, we are far from this limit, and $r \gg Ak_BT/\Delta x^{\ddagger}_{f\to u}$, energy is put into the system faster than it can be dissipated, and $F_u^* > \Delta G^{\ddagger}/\Delta x^{\ddagger}_{f\to u}$.

Although pulling at a fixed loading rate is experimentally possible (23), most unfolding experiments instead have stretched the molecule at a constant speed. Because the stiffness of the molecule depends on the applied force, the loading rate varies as the molecule is stretched and Equation 17 cannot be used directly (22, 24). Instead, values of $k^0_{f\to u}$ and $\Delta x^{\ddagger}_{f\to u}$ are typically determined with the help of Monte Carlo simulations, which mimic the stochastic nature of thermally driven unfolding for a molecule stretched at a constant rate. Values for $k^0_{f\to u}$ are less well determined than those of $\Delta x^{\ddagger}_{f\to u}$ because the former depend exponentially on $\Delta x^{\ddagger}_{f\to u}$ (25, 26). Representative values for F_u (at a particular pulling speed), $k^0_{f\to u}$ and $\Delta x^{\ddagger}_{f\to u}$ are listed in Table 1 for various proteins.

The Unfolding Pathway

Because the location of the transition state along the mechanical reaction coordinate can be determined in these experiments, it should be possible to test for the presence of intermediates along the reaction pathway. In a two-state system, the sum of the distances to the unfolding and refolding transition state should equal to the distance along the unfolding reaction coordinate between native and denatured states:

$$\Delta x^{\ddagger}_{f\to u} + \Delta x^{\ddagger}_{u\to f} = \Delta x_{f\to u}. \quad 20.$$

TABLE 1 Mechanical properties of selected molecules

Molecule	ΔG^0 (kcal/mol)[a]	F_u (pN)[b]	$\Delta X^{\ddagger}_{f\to u}$ (nm)	$k^0_{f\to u}$ (s^{-1})	Structure at "breakpoint"	Reference
dsDNA	1.5–3 (per base pair)	9–20[c]	—	—	DNA base pairs	(110, 111)
P5ab hairpin	37.5 ± 4.8	14.5 ± 0.4[d]	11.9	—	RNA base pairs	(4)
P5abcΔA three-helix junction − Mg^{2+}	34.4 ± 4.8	11.4 ± 0.5[d]	~12	—	RNA base pairs	(4)
P5abc three-helix junction + Mg^{2+}	36.3[e]	19 ± 3 (at 3 pN/s with optical tweezers)	1.6 ± 0.1	2×10^{-4}	Hairpin-bulge	(4)
127 domain from titin (unfolding from native state)	7.6	~100	0.59	1×10^{-6}	Parallel β-sheet shear	(27)
127 domain from titin (unfolding from intermediate)	—	204 ± 26	0.25	3.3×10^{-4}	Parallel β-sheet shear	(112)
128 domain from titin	3.0	257 ± 27	0.25	2.8×10^{-5} or 1.9×10^{-6}	Parallel β-sheet shear	(23, 46)
^{10}FNIII domain from fibronectin	—	74 ± 20	0.38	2.0×10^{-2}	Antiparallel β-sheet shear	(14, 35)
C2A domain	—	60	—	—	β-sheet zipper	(42)
Spectrin	4.8 ± 0.5[f]	25–35 (at 300 nm/s)	1.7 ± 0.5	3.3×10^{-5}	α-helix bundle	(37)
Ubiquitin (N-C linked)	6.7[g]	203 ± 35 (at 400 nm/s)	0.25	4×10^{-4}	β-sheet shear	(38)
Ubiquitin (K48-C linked)	6.7[g]	85 ± 20 (at 300 nm/s)	0.63	4×10^{-4}	β-sheet shear	(38)

[a]From solution measurements, where available. Note that thermodynamic stability ΔG^0 is not a mechanical property, nor does it correlate with mechanical stability, Fu.

[b]All unfolding forces are quoted for pulling speeds in the AFM of 600 nm/s, unless otherwise noted.

[c]Forces obtained vary from 9 pN for AT base pairs to 20 pN for GC base pairs and were the same for optical tweezers and AFM experiments, suggesting that unfolding occurs at equilibrium.

[d]F_u quoted for these secondary structures represents $F_{1/2}$, the force at which the molecule was equally likely to populate the folded and unfolded states. These experiments were done in the optical tweezers under equilibrium, constant force conditions.

[e]Theoretical prediction from Reference 4.

[f]For the α16 domain at 25°C (113).

[g]Reference 114.

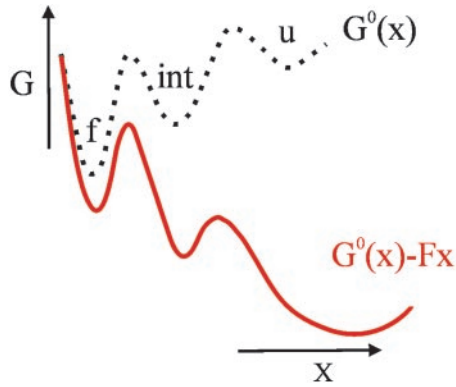

Figure 3 The effect of force on a three-state system, where f, int, and u represent the folded, intermediate and unfolded states of the molecule, respectively. Note how the rate-limiting barrier changes with applied force.

See also Figure 1. The P5ab RNA hairpin (discussed in the previous section), which exhibits no folding intermediates, is described reasonably well by this relation ($\Delta x^{\ddagger}_{f\to u}+\Delta x^{\ddagger}_{u\to f}$ = 11.5 + 11.9 nm = 23.4 nm; $\Delta x_{f\to u}$ = 23 nm). By contrast, a finding of $\Delta x^{\ddagger}_{f\to u} + \Delta x^{\ddagger}_{u\to f} < \Delta x_{f\to u}$ may indicate the presence of intermediates along the reaction pathway. Are there other conditions under which the equality of Equation 20 may not hold? We consider the assumptions that go into determining the distances to the transition state. Equations 13 and 17 assume that the distance to the unfolding transition state from the folded state, $\Delta x^{\ddagger}_{f\to u}$, is independent of force. Because this distance is in general so short and the well and barrier are relatively steep, this is a reasonable assumption. By contrast, the separation between the denatured state and the barrier to refolding, $\Delta x^{\ddagger}_{u\to f}$, is not independent of force, and using the force-dependent refolding kinetics (Equation 13) to determine a fixed value of $\Delta x^{\ddagger}_{u\to f}$ is incorrect (4). This is because the location of the free energy minimum for the unfolded state shifts considerably with force, as described by the worm-like chain equation (2, 3). The distances obtained for P5ab show reasonable agreement with Equation 20 because they were determined over a small range of forces: From 13 to 16 pN, the end-to-end distance of the unfolded RNA chain changes by only 5%, so the distance between the unfolded state minimum and the transition state can be treated as fixed within this force range. Over larger ranges of force, however, this distance cannot be treated as constant.

For reactions that possess intermediates (non-two-state), mechanical unfolding occurs along a complex free energy surface with multiple energetic barriers and may exhibit different rate-limiting transitions in different ranges of force (27, 28). Figure 3 illustrates how force can affect the relative height of barriers along a three-state unfolding reaction coordinate. The energies and locations of the transition state barriers and of the intermediate structure strongly influence the

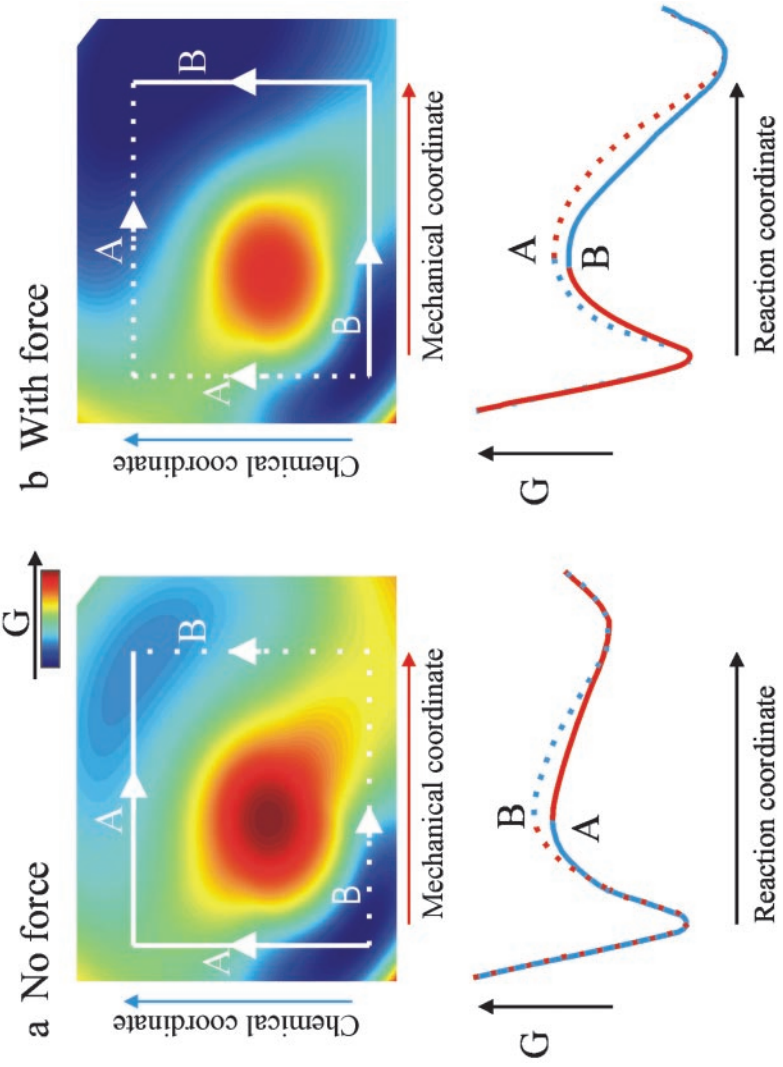

unfolding pathway of a molecule under force, since force reduces the free energy to a greater extent at positions further along the mechanical reaction coordinate than at positions closer to the folded structure. By mechanically unfolding mutant and wild-type I27 domains, and carefully analyzing the unfolding kinetics within the constraints of a three-state system, Clarke and coworkers identified distinct unfolding pathways in three different force ranges (27, 29). At high forces, an intermediate state is rapidly attained and unfolding occurs from this state; at lower forces, unfolding occurs directly from the native state; and at forces below ~43 pN, unfolding follows a distinct "solution" pathway that has a different (lower-energy) transition state than the mechanical transition state. This study demonstrates the difficulties inherent in extrapolating unfolding rates to zero force.

How are the results of mechanical unfolding experiments related to those of bulk unfolding experiments? Thermodynamic properties such as the free energy of unfolding are state functions and depend only on the initial and final states of a process; thus, comparisons between single-molecule mechanical studies and bulk biochemical assays should give identical results (after correcting for the entropic contribution of tethered ends). The kinetics of a reaction is, however, pathway dependent. Because single-molecule unfolding experiments impose a reaction coordinate different from that of bulk experiments, rates of unfolding obtained with these two different approaches will generally differ. Figure 4 illustrates the effect of force on a two-dimensional free energy surface, where one of the axes represents the mechanical reaction coordinate and the other an orthogonal "chemical" coordinate. From this simple depiction, it is clear how the unfolding pathway can change with force: an applied force lowers the high-energy barrier located far along the mechanical reaction coordinate. Above a given force, this barrier becomes lower than the rate-limiting barrier at zero force (which is not located along the mechanical coordinate and is unaffected by force), creating a more energetically favorable trajectory. Thus, under the influence of mechanical force, the unfolding reaction may follow an entirely different trajectory than it does when free in solution (5, 27, 30), as the barrier to unfolding along the mechanical pathway becomes lower in free energy than the chemical barrier.

Figure 4 Force can affect the reaction pathway along a two-dimensional free energy surface. Two paths (*A* and *B*) are shown connecting the folded state minimum (*lower left*) to the unfolded state minimum (*upper right*) of the free energy contour plot; the preferred path is indicated by the solid line. The lower panels illustrate the free energy along these paths, where blue sections occur along the chemical coordinate and those in red occur along the mechanical coordinate. (*a*) No applied force: the reaction following pathway *A* encounters a lower activation barrier than the reaction following pathway *B*. (*b*) An applied force tilts the free energy surface along the mechanical coordinate, lowering the barrier along pathway *B* below the barrier along pathway *A*.

Relating Mechanical Stability to Local Molecular Structure

The mechanical unfolding pathways of RNA and proteins are fundamentally different. Complex RNA structures unfold in a hierarchical manner, with stable secondary domains remaining after tertiary interactions have ruptured. This hierarchical behavior is rooted in the separability between the energy contributions from the secondary interactions of each individual subdomain and the contribution of its tertiary contacts (4, 31, 32). In other words, secondary and tertiary interaction energies are independent and additive, and coupling energy terms can be neglected, to a first approximation:

$$\Delta G = \Delta G_{2^\circ} + \Delta G_{3^\circ} (+\Delta G_{coupling}) \qquad 21.$$

In agreement with this analysis, single-molecule mechanical unfolding experiments have shown that a given secondary RNA domain exhibits the same distribution of unfolding forces and lengths in isolation as when it is involved in tertiary interactions in a larger molecule, meaning that kinetic barriers associated with isolated structural subdomains are maintained within the larger molecule (32). Thus, by pulling on progressively larger pieces of the *Tetrahymena thermophila* L21 ribozyme, it was possible to map completely the unfolding pathway of the molecule (32). Because tertiary structures have shorter distances to their transition states than secondary structures, tertiary interactions tend to be brittle (they break at high forces after small deformation), whereas secondary interactions are compliant (they break at low forces and after large deformations) (4). In addition, tertiary interactions equilibrate over a slower timescale than secondary interactions and their presence is more often than not accompanied by hysteresis in the pulling-relaxation cycle. By pulling the ribozyme many times, it was possible to identify the alternative unfolding pathways of the molecule and their relative probability of occurrence (32). The approach described above suggests that by characterizing the interaction energies of the various tertiary motifs (helix-helix, kissing loops, loop-helix, etc.) it should be possible to develop an *Aufbau* algorithm to solve the RNA folding problem, i.e., to predict the tertiary structures of RNA molecules from their sequence using a semiempirical approach (31): First the most probable secondary structure is predicted from the sequence, and this structure is then used to predict its most probable tertiary fold.

In contrast to RNA, proteins appear to unfold in a highly cooperative manner, and secondary structures are not stable independently of their tertiary context. Mechanical unfolding intermediates have been identified for a few proteins (33–36), in which most intermediate structures involve little disruption of the core domain of the protein, and instead involve peeling off a single external β-strand from a large β-barrel or β-sandwich structure. In the immunoglobin I27 domain, for example, low forces break two hydrogen bonds between outlying antiparallel β-strands, while the core of the protein domain remains folded until higher forces are attained (27, 33). The cooperativity of protein unfolding most

likely arises from the high degree of connectivity involved in the interactions that maintain protein structure.

As seen in Table 1, mechanical stability (given by the most probable unfolding force, F_u^*) is not correlated with thermodynamic stability (ΔG), nor can it be predicted from the melting temperature ($T_m = \Delta H/\Delta S$) (35, 37–39). Instead, as predicted by Equation 17, the mechanical stability of the molecule depends on the location of the transition state along a specific mechanical reaction coordinate, the height of the barrier (which contributes to k_u^0), and the loading rate. As discussed earlier, force affects most strongly positions furthest from the folded, native state: To mechanically eliminate a 10-k_BT barrier located 0.3 nm from the folded state requires ~140 pN of force (when the molecule is stretched under conditions of quasi-static equilibrium), whereas to eliminate a barrier of the same height but located 1.5 nm from the folded state along the mechanical reaction coordinate requires only 28 pN under the same conditions. Many mechanical proteins consist of tandem arrays of domains with different transition state locations and hence differing mechanical stability. The more compliant domains (having longer distances to their transition states) stretch in response to low applied forces, while the more brittle domains (with shorter distances to their transition states) maintain their structure to higher applied forces and only under extreme force conditions would they unfold (35, 36).

The molecular structure provides physical insight into the location of the transition state barrier along the mechanical reaction coordinate. Proteins that contain β-sheets tend to unfold at much higher forces and exhibit less compliance than proteins that are predominantly α-helical (see Table 1) (40). Gaub and coworkers have suggested that this trend can be explained in broad terms by the difference in forces maintaining tertiary structure (37): β-barrel domains are held together by intrasheet hydrogen bonds, which are short-range interactions with short distances to their transition state, whereas tertiary interactions maintaining α-helical bundles are hydrophobic, are more delocalized, and have associated longer distances to their transition state. However, due to the local action of applied mechanical force, the unfolding force is most strongly influenced not by global domain structure but by the local structure near the mechanical "breakpoint."

The strongest protein domain examined thus far, the I27 immunoglobin domain from titin, has a β-sandwich structure. Structural considerations, molecular dynamics simulations, and mutational analysis have been combined to demonstrate that the mechanical breakpoint of this domain at the strongest applied forces consists of a cluster of six hydrogen bonds between parallel β-strands experiencing shear forces (33, 41). Not only is the energy barrier for breaking many bonds in a concerted fashion much greater than the individual energy barriers for breaking individual bonds sequentially, but the stiffness of the connection between the two strands is also greater for shearing six parallel hydrogen bonds than for breaking a single bond (or six bonds in series). The higher transition-state energy barrier requires greater forces to lower it; the

increased stiffness implies steeper walls about the native state free energy minimum, which result in a shorter distance to the transition state for the concerted versus sequential cleavage of six hydrogen bonds. Similarly short distances to the transition state were found for other domains experiencing shearing forces between clusters of hydrogen bonds (Table 1). By contrast, sequential breakage of single hydrogen bonds, occurring when β-strands of a protein are "unzipped" or when an RNA hairpin is mechanically unfolded, requires lower energy, and because the potential energy well is shallower, the transition state is located at a longer extension. The result is that sequential cleavage of multiple bonds requires less energy and applied force than concerted cleavage of the same set of bonds. Accordingly, while the structure at the mechanical breakpoint is important for mechanical stability, the direction of applied force can significantly change the force at which the breakpoint ruptures (38–40, 42, 43).

Extending Single-Molecule Mechanical Properties to the Cellular Level

The results of mechanical experiments on individual domains of titin, on single molecules of the entire protein, and on the muscle sarcomere illustrate the convergence, and in some cases complementarity, of information obtained by studying the mechanical properties of proteins at an increasing level of complexity. The similarity of the force-extension curves of single molecules of titin and of the sarcomere (when extrapolated to the single-molecule level) confirm that single-molecule experiments on titin reproduce the physiological elastic response of muscle (36, 44, 45). Muscle elasticity can be described at a still more fundamental level: By determining the mechanical unfolding properties of its individual domains, Fernandez and coworkers have reconstructed the force-extension curve of the complete titin molecule (36). They attribute muscle elasticity at low force (< 4 pN) to the compliance of titin's PEVK and N2B regions, while the inclusion of the more brittle Ig domains in the tandem array provides titin the "mechanical buffer" necessary to react to potentially damaging higher forces or to forces applied for long periods of time (36).

The ability to predict, from studies of individual protein domains, the mechanical behavior of the entire molecule suggests that, to a first approximation, the domains of titin can be treated as independent structural entities. This result appears to be true for most domains of tandem proteins, in which the mechanical unfolding properties of individual domains are independent of their neighbors. Some domains, however, exhibit different unfolding behavior depending on their context within a tandem array (35, 46, 47). Although the characterization of individual domains provides valuable information on the mechanical properties of the parent protein, the mechanical behavior of the entire molecule must also be studied to determine the role of interdomain interactions and other sources of higher-order behavior. By repeatedly stretching both individual titin molecules and the muscle sarcomere, for example, Kellermayer et al. observed

mechanical fatigue, where the system became more compliant and extended to greater lengths on consecutive pulls (45). This behavior has not been observed in studies of individual domains of titin, and Kellermayer et al. attribute it to nonspecific intrachain crosslinks, suggesting that the physiological significance of fatigue may be to dynamically modulate the mechanical properties of the muscle in response to its recent mechanical history (45). These studies on the sarcomere, titin, and its constituent domains demonstrate how careful experiments on systems of varying degrees of complexity can provide insight into the physiological mechanical behavior of proteins.

MOLECULAR MOTORS

Introduction

To carry out processes as diverse as cell movement, organelle transport, ion gradient generation, molecular transport across membranes, protein folding and unfolding, and others, cells possess molecular structures that behave as tiny machine-like devices. These molecular machines must use external energy sources to drive directed motion and operate as molecular motors, converting chemical energy into mechanical work.

The myosin, kinesin, and dynein families of molecular motors, whose best-characterized members are most closely associated with muscle contraction, organelle transport, and ciliary beating, respectively, use ATP hydrolysis as a source of energy to step along a track—actin filaments, in the case of myosin, or microtubules, for kinesin and dynein. In replication, transcription, and translation, molecular motors must utilize part of the chemical energy derived from the polymerization reaction to move along the DNA or RNA in a unidirectional manner, generating forces and torques against hydrodynamic drag and/or mechanical roadblocks (48, 49). Many other enzymes that bind to and act on DNA or RNA are molecular motors. Helicases hydrolyze ATP to translocate along DNA, unwinding it into its complementary strands (50, 51). Type II topoisomerases exert forces to pass DNA duplexes through double-strand breaks in DNA and to reseal these breaks (52–54). Many protein translocases are also likely to operate as molecular motors using ATP hydrolysis to mechanically pull polypeptide chains across membranes (15). Finally, during the replication cycle of many dsDNA bacteriophages and viruses, a molecular motor must package the DNA of the virus into newly self-assembled capsids against considerable entropic, electrostatic, and elastic forces (55). Motors not only move along linear tracks (microtubules, polymerized actin, DNA, RNA, or polypeptide chain) exerting forces, but can also operate in a rotary fashion, generating torque. F_1F_0 ATP synthase and the motor at the base of the prokaryotic flagellum utilize the electrochemical energy of a transmembrane proton gradient to generate torque and synthesize ATP, and to propel the bacterium, respectively (56, 57).

Many approaches have been used to study the mechanisms of molecular motors. Structural studies provide detailed information on the various conformations of the motor, but these pictures are static. Biochemical assays of motility and kinetics provide a more dynamic picture, yet they involve averages over large numbers of molecules. Because molecular populations are often heterogeneous, the ensemble-averaged properties measured in these studies may not be representative of individual molecules. The recent development of single-molecule techniques has made it possible to probe the individual molecules that make up the ensemble and, for the first time, allow direct determination of intrinsic molecular motor properties such as efficiency, stall force, and motor step size. In the following section, we discuss in detail the significance of these properties.

Mechanical Properties of Molecular Motors

EFFICIENCY AND COUPLING CONSTANT All molecular motor reactions are exergonic ($\Delta G < 0$), meaning that they occur energetically "downhill." The free energy ΔG that drives the mechanical motion is derived from chemical sources, for instance, the energy of ATP hydrolysis, the electrochemical energy from a transmembrane ion gradient, or the polymerization energy derived from bond breaking and forming in DNA, RNA, or polypeptides. As in the case for mechanical unfolding, it is possible to define an efficiency—a ratio of output work to input energy—of a molecular motor. The thermodynamic efficiency η_{TD} of a motor is defined as the ratio per step between the work done by the motor against a conservative external force[2] and the free energy associated with the reaction that powers the motor, ΔG: $\eta_{TD} = F\delta/\Delta G$. Here, F is the external mechanical force and δ is the step size of the motor (see below for more on step size). The thermodynamic efficiency must be less than unity, since the motor cannot, on average, do more work than the free energy supply ΔG it is given. Furthermore, since η_{TD} increases with the force, it follows that the motor attains its highest efficiency at the maximum force against which it can work. As discussed below, at this force the motor stalls.

Table 2 lists the thermodynamic efficiencies of a few molecular motors at stall.[2] The values vary between 15% to 100%. The observed variation in molecular motor efficiency may reflect the large uncertainties still associated with the determination of the stall force and the step size using methods of single-molecule manipulation (see below). An observed mechanical efficiency $<100\%$ suggests that part of the energy of the reaction is either dissipated as heat or utilized to perform work along a reaction coordinate orthogonal to the direction of the applied mechanical load. RNA polymerases, for example, may

[2]A distinction must be made between the case in which the motor works against a conservative force and a dissipative viscous force. The efficiency of the F_1-ATPase (70) was determined from experiments in which the rotary motor operated against the viscous drag of a long actin filament. Here, a different efficiency from that described above must be used: the Stokes efficiency (121).

TABLE 2 Mechanochemical properties of a few molecular motors

Motor	Average speed (nm/s)	Average stall force (pN)	Step size (nm)	Efficiency[a]
F_1-ATPase[b]	4 rps[h]	40 pN·nm	120°	100%
RNA polymerase[c]	6.8	15–25	0.34	9–22%
DNA polymerase[d]	38	34	0.34	23%
Myosin II[e]	8000	3–5	5.3	12–40%
Kinesin[f]	840	7	8	40–60%
Phage ϕ29[g]	34	57	0.68	30%

[a]Calculated from $F_{stall}\cdot\delta/\Delta G$ where δ is the (putative) step size, and ΔG is the free energy change for the reaction.
[b]References 70, 115.
[c]The step size of RNA polymerase has not been measured directly but is expected to be one base pair (64, 74).
[d]The step size of DNA polymerase has not been measured directly but is expected to be one base pair (49).
[e]References 66, 116–118.
[f]The stall force for kinesin can vary between 3–7 pN (63, 119, 120).
[g]The step size of ϕ29 has not been measured directly but is thought to be two base pairs (55, 72).
[h]Revolutions per second (rps).

have the ability to generate torque to overcome the torsional stress built up in the DNA molecule during transcription. The packaging motor in bacteriophage ϕ29 may use part of the energy to twist the DNA and facilitate its arrangement inside the capsid.

A related concept that quantifies the conversion of chemical energy into mechanical motion is the coupling constant ξ, defined as the probability that the motor takes a mechanical step per chemical reaction. If one step is taken per catalytic cycle ($\xi = 1$), the motor is tight coupled; if less than one step is taken ($\xi < 1$), the motor is loose coupled. Still other coupling mechanisms may exist in which many steps are taken per catalytic cycle ($\xi > 1$), so-called one-to-many coupling schemes.

There is no simple correspondence between the coupling ξ and efficiency η. A motor could be tight coupled but have a low efficiency, as appears to be the case for kinesin (58, 59). In principle, a loose-coupled motor could also have a high efficiency. In other words, a motor may step only once per several chemical reactions, but when it does, utilizes all of the chemical energy available to it.

STALL FORCE The stall force of a molecular motor, F_{stall}, is the force at which the velocity of the motor reduces to zero, and thus it is equal to the maximum force that the motor itself can generate during its mechanical cycle. Stall forces vary greatly from motor to motor (Table 2), depending on the motor's speed of operation and step size, which are ultimately dictated by its biological function. For example, during transcription elongation, RNA polymerases must locally unwind the DNA template, work against torsionally constrained DNA, and possibly disrupt protein roadblocks such as nucleosomes that impede its trans-

location. To perform these tasks, *Escherichia coli* RNA polymerase generates forces up to 25 pN (48, 60), sufficient to mechanically unzip dsDNA (~15pN; see Table 1). The connector motor at the base of bacteriophage ϕ29's capsid, on the other hand, must pack the phage DNA in the capsid against the build-up of an internal pressure that reaches a value of nearly 6 megaPascals (MPa) at the end of packaging. To perform this task, the motor is capable of exerting forces as high as ~60 pN (55).

What factors influence the stall force? The stall force is that at which the transition of a motor between states at sequential positions along its track occurs at equilibrium. In other words, the motor oscillates between these states (A and B) so that the net displacement is zero. Because A and B represent sequential positions along a periodic track, the local curvatures of the free energy surface at these positions are identical, in contrast to those of an unfolding molecule (see previous section). As a result, Equation 7 can be used to determine the external opposing force that stalls the motor (see 61):

$$F_{stall} = \frac{\Delta G^0}{\delta} + \frac{k_B T}{\delta} ln \frac{[B]}{[A]}. \qquad 22.$$

[*A*] and [*B*] are the populations of states A and B, respectively, ΔG^0 is the standard free energy of the reaction, and δ is the distance translocated along the track: the step size of the motor (see below). Thus, for given values of ΔG^0, [*A*] and [*B*], the smaller the step size, the larger the force required to stall the motor. Implicit in Equation 22 is the assumption that the motor is 100% efficient. Indeed, this expression represents the maximum stall force; if the motor utilizes only a fraction of the reaction free energy, Equation 22 should be scaled accordingly. Because the magnitude of the stall force depends on the relative populations of states A and B, albeit in a weak manner, it is important to specify the concentrations of products and reactants under which the stall force was determined. For a motor that hydrolyzes ATP, for instance, [*B*]/[*A*] in Equation 22 is replaced by $[ADP][P_i]/[ATP]$. A dependence of the stall force on product and reactant concentrations was observed for kinesin (62, 63), but not for *E. coli* RNA polymerase (48, 64).

When the population of state B is zero (equivalently, when the product concentration is zero), Equation 22 predicts an infinite stall force. Because the reaction is now irreversible, the motor can never step backward, even under a large force. The motor will wait until it experiences a thermal fluctuation large enough to carry it forward. As a result, the velocity becomes exponentially small at high forces, but will remain positive. In practice, however, there is little experimental distinction between an exponentially small and a zero velocity. Thus, many measurements of the stall force likely underestimate the true stall force (as well as the efficiency), as formally defined in Equation 22. Ultimately, at high enough forces, the motor or its track will deform, rendering it inactive.

If the reaction is reversible such that the stall force is finite, a motor can in principle be run backward, turning products into substrate, by applying sufficiently large forces. A possible example of this is ATP synthase in which the direction of rotation of the F_1 motor—by itself an ATPase—is thought to be reversed by the counter-rotating F_0 motor in order to drive ATP synthesis (65). The mechanical reversibility of the F_1 motor has recently been demonstrated in elegant experiments by Kinosita and coworkers (65a). They mechanically counter-rotated the F_1 motor and found that the hydrolysis reaction was also reversed, synthesizing ATP from ADP and P_i. The work required to reverse a molecular motor must clearly equal or exceed the free energy of the reaction. If a motor is 100% efficient, reversal occurs at forces just beyond the stall force as defined in Equation 22, infinitely slowly, but with 100% efficiency. At larger forces, the process is faster but less efficient.

STEP SIZE The step size, δ, of a motor is defined as its net displacement during one catalytic cycle (see Table 2). Clearly, the step size is best determined from direct observations. Several groups have employed single-molecule techniques to observe individual steps of myosin II (66, 67) and kinesin (68) that compare well to the known periodicity of their tracks (5.5 nm for actin filaments, 8 nm for microtubules). Recent experiments (69) suggest that the 8-nm displacement of kinesin is comprised of two smaller substeps. However, hydrolysis of one ATP molecule drives the motor the entire 8-nm distance (58, 59).

As discussed above, the distance between two states can vary with force in a manner that depends on the local curvatures of the free energy surface. Because the motor's track is periodic, we expect sequential positions to have identical free energy curvatures, and thus, we expect the step size to be independent of force. This prediction has been confirmed in the case of kinesin (69) and F_1-ATPase (70, 71).

In many cases, the step size has not been observed directly. The difficulty lies in the extraordinary spatial resolution required to make such observations. Optical trap techniques do not currently have sensitivity sufficient to resolve subnanometer displacements. Nevertheless, thermodynamic arguments can be made to place an upper bound on the step size. Since the thermodynamic efficiency of a motor must be less than 100%, from the free energy of NTP binding and hydrolysis and the measured stall force a maximum allowable step size of $\sim$2 basepairs (1 bp = 3.4Å) can be estimated for RNA polymerase (48). For the packaging motor of bacteriophage ϕ29, arguments based on motor efficiency and single-molecule measurements of the maximum stall force ($\sim$70pN) suggest that the step size must be smaller than $\sim$5 base pairs (55). One biochemical bulk study that measured the amount of DNA packaged and ATP hydrolyzed suggests that the movement is $\sim$2 bps per ATP (72).

Mechanochemistry

The distinguishing feature of a molecular motor is the generation of force to produce the mechanical motion that accompanies the reaction. How motors

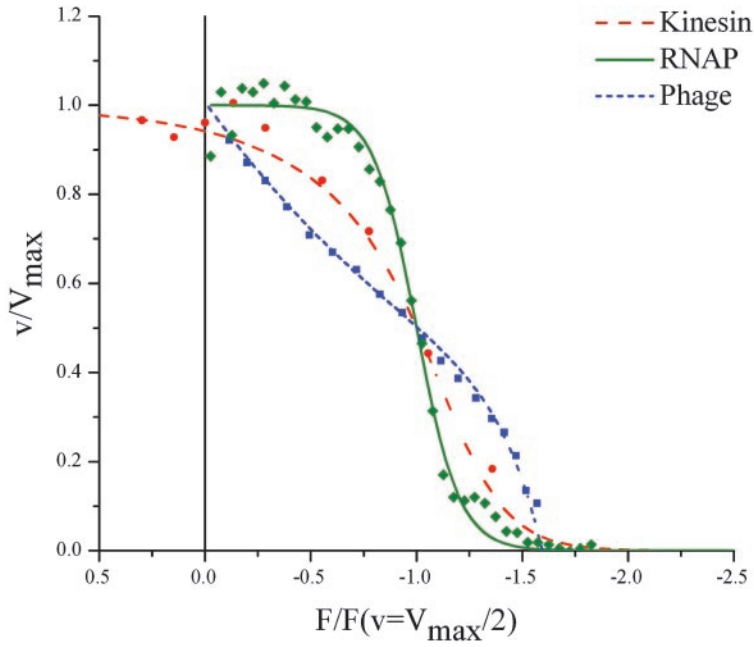

Figure 5 Force-velocity behavior for kinesin (73), RNA polymerase (48), and the bacteriophage ϕ29 packaging motor (55) under saturating conditions. Data were normalized in order to appear on the same graph. Velocities are scaled to their maximum values, and forces are scaled to those at which the velocities are half-maximal, $F(v=V_{max}/2)$. The different shapes of the force-velocity curves imply distinct mechanisms.

convert chemical energy into mechanical movement—the mechanochemistry of the motor—is discussed in this section. In a sense, force can be considered a product of the chemical reaction. Thus, an external force that opposes the motor can function as an inhibitor of the reaction, and one in the aiding direction can promote the reaction and act as an activator. As a result, the velocity of the motor often depends on the external force and does so in a manner dictated by the mechanism of motor operation. Force-velocity behavior can thus provide much insight into a motor's mechanochemical conversion. In general, the shape of the force-velocity relationship will vary depending on the conditions (concentration of reactants and products of the hydrolysis reaction) under which the motor is tested. The rate of a molecular motor will be force dependent if the conditions of the experiment are such that movement itself is the rate-determining step.

Figure 5 shows the normalized force-velocity behavior of three molecular motors—kinesin (73), phage ϕ29 DNA packaging motor (55), and *E. coli* RNA polymerase (48)—at saturating substrate concentrations. The range in behavior among motors is striking, and hints at the underlying differences in their

respective mechanisms. The velocity of the ϕ29 packaging motor decreases linearly with force over practically the entire range of forces, suggesting that the rate-limiting step of the reaction, in the conditions in which the data were obtained, is DNA translocation, even at low forces. Kinesin exhibits similar behavior, with somewhat less force dependence at low forces than near stall. The velocity was practically independent of force when a constant force was applied assisting the movement of kinesin, suggesting that the rate-limiting step is not translocation for assisting forces (73). In marked contrast to those enzymes, the velocity of RNA polymerase is practically force independent, except near stall, indicating that the movement step is not the rate-limiting step in this case.

The force-velocity relationship of a molecular motor under various concentrations of substrate and its hydrolysis products provide quantitative information about the mechanochemical cycle of the motor. This cycle consists of catalytic steps that connect distinct chemical states and mechanical steps that connect different conformational states. A reaction pathway may typically include a substrate binding step, reaction steps, product release steps, and mechanical steps (which may coincide with chemical steps). Provided the reaction is irreversible (as when the product concentration is zero, for instance), the rate k_t at which the enzyme turns over is given by an expression with the general form of the Michaelis-Menten Equation:

$$k_t = \frac{k_{cat}[S]}{K_M + [S]}, \qquad 23.$$

where $[S]$ is the substrate concentration, and where k_{cat}, the maximum rate in units of moles·sec^{-1}, and K_M, the Michaelis constant, are determined by the individual transition rates connecting the various states of the motor during its mechanochemical cycle (see below). The velocity of the motor is simply given by $v = \xi\delta{\cdot}k_t$, where δ is the step size of the motor, and ξ is the coupling constant (which we assume is 1 for the following discussion).

Force-velocity curves alone cannot reveal the location of the movement step in the cycle of the motor. As is illustrated below, it is necessary to determine the force dependence of the parameters of the Michaelis-Menten Equation, $V_{max} = \delta{\cdot}k_{cat}$ and K_M (61). Consider a general N-step kinetic scheme with two irreversible steps,

$$M_1 + S \underset{k_{\pm 1}}{\longleftrightarrow} M_2 \underset{k_{\pm 2}}{\longleftrightarrow} \ldots M_j \xrightarrow[k_j]{} M_{j+1} \underset{k_{\pm(j+1)}}{\longleftrightarrow} \ldots M_N \xrightarrow[k_N]{} M_1 \qquad 24.$$

where step 1 is the substrate binding step. Because the cycle is irreversible, the velocity obeys the Michaelis-Menten Equation 23. At saturating substrate levels ($[S] \gg K_M$), the velocity $v \sim V_{max} = \delta{\cdot}k_{cat}$ is independent of substrate. At low concentrations ($[S] < K_M$), the velocity is limited by substrate binding: $v \sim V_{max}[S]/K_M = \delta{\cdot}k_{cat}/K_M[S]$, where k_{cat}/K_M is an effective second-order binding rate constant. It can be shown that for the scheme in Equation 24, V_{max} is a function of all rate constants $k_{\pm 2}$, $k_{\pm 3}$,. . . k_{N} except rate constants $k_{\pm 1}$

TABLE 3 Dependence of parameters from the Michaelis-Menten Equation on opposing force

Case	Force-dependent rates	V_{max}	k_{cat}/K_M	K_M
1	$k_{\pm 1}$	–	↓	↑
2	$k_{\pm(j+1)}, k_{\pm(j+2)}, \ldots, k_N$	↓	–	↓
3	$k_{\pm 2}, k_{\pm 3}, \ldots, k_j$	↓	↓	↓ or ↑

associated with the substrate binding step. On the other hand, k_{cat}/K_M depends on all of the rate constants that connect enzyme states reversibly to substrate binding (step 1), and on the forward rate for the first irreversible step that follows binding, k_j (i.e., $k_{\pm 1}$, $k_{\pm 2}$,. . . k_j).

An interesting consequence of this result is that the location of a force-dependent step in the cycle dictates how the parameters V_{max} and k_{cat}/K_M are affected by force (see Table 3). There are three possible cases depicted in Figure 6 for a simplified reaction cycle, which are discussed below.

THE MOVEMENT STEP COINCIDES WITH BINDING ($k_{\pm 1}$). This case results in a force-dependent k_{cat}/K_M and a force-independent V_{max}. Here, an opposing force acts like a competitive inhibitor to the substrate, shifting the equilibrium toward the free enzyme state (M_1), reducing the effective binding rate constant k_{cat}/K_M. However, the addition of more substrate outcompetes this effect, shifting the equilibrium back to the substrate-bound state (M_2). As a result, the velocity at infinite substrate concentration, V_{max}, is unaffected by force. K_M increases with opposing force as more substrate is necessary to counteract the effect of force.

Figure 6 Schematic representation of the free energy surface of a molecular motor along a generalized reaction coordinate. Sections marked in blue occur along a chemical coordinate and are independent of force; those in red occur along the mechanical coordinate, and hence depend on force. We assume that the force-dependent step is rate-limiting in each case. For simplicity, we consider the minimal three-state kinetic cycle

$$M + S \underset{k_{\pm 1}}{\longleftrightarrow} M \cdot S \underset{k_2}{\longrightarrow} M \cdot P \underset{k_3}{\longrightarrow} M + P,$$

in which substrate binding is followed by two irreversible steps (depicted by two large free energy drops). The effective second-order binding rate k_{cat}/K_M is the rate at which the motor reaches the state M·P through the first two steps. Once in that state, the motor is committed to proceeding forward, so that binding cannot be affected by any subsequent transition. V_{max}, on the other hand, depends on the second and third transitions, which are independent of substrate concentration. (*a*) In case 1, the first step is force dependent; k_{cat}/K_M decreases with force, whereas V_{max} is force independent. (*b*) In case 2, the third transition is force dependent; V_{max} decreases with force, and k_{cat}/K_M is force independent. (*c*) In case 3, the second step is force dependent; both k_{cat}/K_M and V_{max} decrease with force.

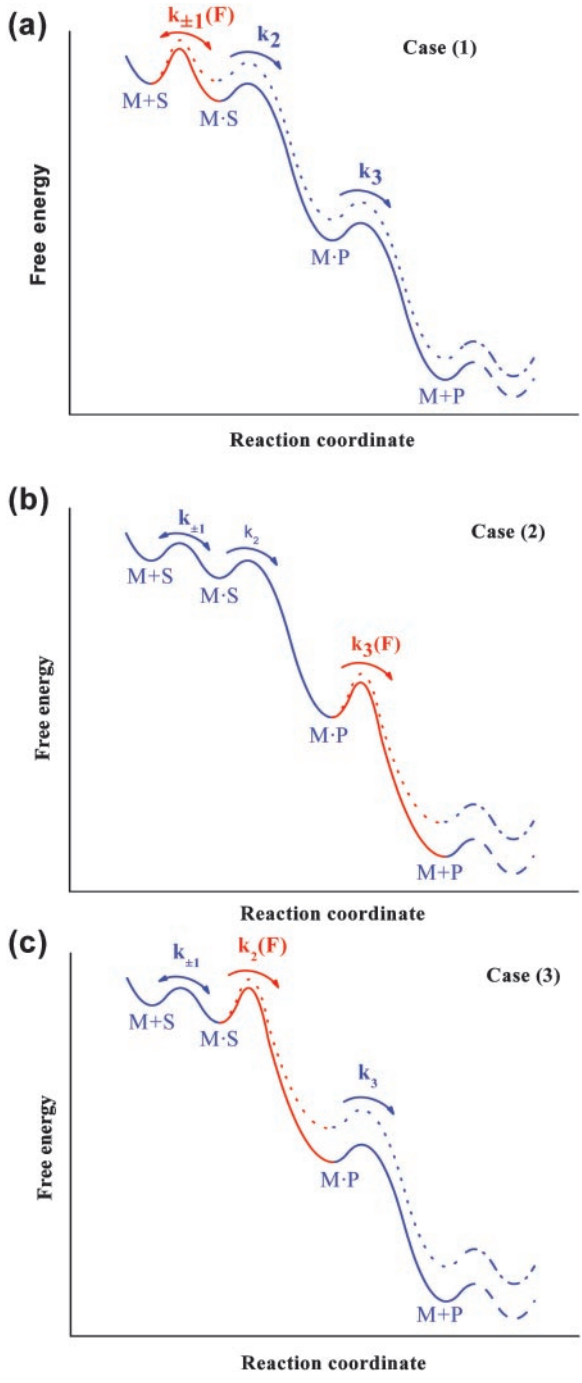

Recent experiments have shown that the force-velocity behavior of T7 RNA polymerase is consistent with a force-dependent rate-limiting step at subsaturating NTP concentrations (75). This motor exhibits a force-independent velocity V_{max} at forces below stall, while K_M increases with opposing force (75). Thus, T7 RNA polymerase appears to follow case 1. The authors have proposed a model for translocation in which the movement step occurs in equilibrium with NTP binding, and hydrolysis and incorporation of NTP serve to rectify translocation in a unidirectional manner.

THE MOVEMENT STEP FOLLOWS THE FIRST IRREVERSIBLE STEP AND PRECEDES THE NEXT BINDING EVENT ($k_{\pm(j+1)}$, $k_{\pm(j+2)}$,... k_N). In this case, the force dependence is reversed: V_{max} depends on force, k_{cat}/K_M does not. An opposing force affects the equilibrium between states not connected to substrate binding, like an uncompetitive inhibitor. As a result, when substrate binding is rate-limiting ($[S]<K_M$), the velocity ($v \sim \delta \cdot k_{cat}/K_M[S]$) does not depend on force. In the other extreme ($[S] \gg K_M$), the velocity ($v \sim V_{max}$) is reduced by an opposing force, provided the force-dependent step (translocation) is rate-limiting. Note that K_M must have the same force-dependence as V_{max} in this case to yield a force independent k_{cat}/K_M.

As discussed previously, the force-velocity behavior of the ϕ29 packaging motor at saturating ATP indicates that the rate-limiting step is force dependent. At limiting ATP concentrations, however, it was found that the velocity is practically independent of force except close to stall (Y.R. Chemla, A. Karunakaran, J. Michaelis & C. Bustamante, unpublished data). Measurements of V_{max} and K_M from the ATP dependence of the velocity at various forces show that both decrease with opposing force in the same manner, such that k_{cat}/K_M is force independent (Y.R. Chemla, A. Karunakaran, J. Michaelis & C. Bustamante, unpublished data). Thus, ϕ29 appears to follow case 2. A putative minimal kinetic scheme for this motor can then be proposed:

$$M_1 + ATP \underset{k_{\pm 1}}{\longleftrightarrow} M_2 \underset{k_2}{\longrightarrow} M_3 \underset{k_3(F)}{\longrightarrow} M_4 \underset{k_{\pm 4}}{\longleftrightarrow} M_5 \underset{k_{\pm 5}}{\longleftrightarrow} M_1.$$

The movement step (step 4) occurs after product release.

THE MOVEMENT STEP OCCURS AFTER BINDING IN ANY STEP UP TO AND INCLUDING THE FIRST IRREVERSIBLE STEP ($k_{\pm 2}$, $k_{\pm 3}$,... k_J). In this case, force affects the equilibrium between states indirectly connected to binding, so that both V_{max} and k_{cat}/K_M are force dependent. Here, an opposing force acts essentially as a mixed (noncompetitive) inhibitor. It favors the free enzyme state, reducing the effective binding rate k_{cat}/K_M (as in case 1), but cannot be outcompeted with substrate, so that V_{max} is still reduced (as in case 2). Note that depending on the relative strengths of V_{max} and k_{cat}/K_M, K_M may increase or decrease as a function of force.

Two experiments by Block and coworkers (63, 73) have shown that for kinesin V_{max} and k_{cat}/K_M decrease with opposing force, whereas K_M increases,

consistent with case 3. [By contrast, Nishiyama et al. (69), in an experiment based on measuring times between kinesin steps, did not observe any force dependence of K_M.] For assisting forces, other transitions in the cycle are rate-limiting, and little force dependence is observed in V_{max} and k_{cat}/K_M. As a result of these findings, Block et al. (73) have proposed the following minimal reaction pathway for kinesin:

$$M_1 + ATP \underset{k_{\pm 1}}{\longleftrightarrow} M_2 \underset{k_{\pm 2}(F)}{\longleftrightarrow} M_3 \underset{k_3}{\longrightarrow} M_4 \underset{k_4(F_1)}{\longrightarrow} M_5 \underset{k_5(F_1)}{\longrightarrow} M_1.$$

Step 2 is the primary movement step and is rate-limiting for opposing forces. For assisting forces, step 3 is rate-limiting. Steps 4 and 5 are weakly dependent on forces applied perpendicularly to the direction of motion and only affect the maximum velocity V_{max}, not the effective binding rate k_{cat}/K_M. Furthermore, by studying the effect of force on ADP binding to kinesin, Uemura et al. (76) showed that assisting force increases the binding affinity of the motor for ADP, whereas an opposing force decreases it. This observation strongly suggests a reciprocal coupling between the direction of force (whether assisting or opposing) and the enzymatic activity of the motor. The release of ADP increases the binding affinity of the kinesin head to the microtubule (77). Uemura et al. (76) postulate that an internal strain may modulate the binding affinity for ADP and hence may control the motor's processivity.

One of the movement steps of F_1-ATPase occurs during binding of ATP (78). Although this appears consistent with case 1, experiments show that V_{max} decreases with torque, an observation more consistent with cases 2 and 3 (70). The reason for this discrepancy is that our treatment of ATP binding as a single-step, second-order process is an oversimplification of the true binding mechanism. More generally, binding may consist of a second-order "docking" process in which the substrate comes into loose contact with the binding site, followed by one or more first-order "accommodation" steps in which it becomes progressively more tightly bound to the enzyme. Provided these docking steps are reversible, this situation is analogous to case 3. An illustration of this more complex mechanism is precisely the "binding zipper" in F_1-ATPase, in which ATP binding to the catalytic site has been postulated to occur via a zippering of hydrogen bonds, generating a constant torque (79). This example illustrates the need to exercise caution when generating mechanistic models. Force measurements at various ATP, ADP, and P_i concentrations often need to be supplemented with kinetic measurements and structural data to form a complete and accurate picture of motor mechanism.

STRAIN IN ENZYME CATALYSIS

Introduction

In the previous section, we have seen that molecular motors have evolved as energy transducers to convert chemical energy into mechanical work. Binding

energy represents a ubiquitous but otherwise "silent" form of energy in the cell that can be considered as one of the main sources of potential energy to perform various molecular tasks. In this section, we generalize the idea of the energy transducer and discuss how the binding energy between an enzyme and its substrate can be utilized to accelerate the rate of chemical reactions.

Chemical catalysis is essential for many critical biological processes to proceed at useful rates under physiological conditions. Thus, a molecular description of the mechanisms by which an enzyme achieves high catalytic efficiency is of crucial importance to understand the control and coordination of the complex biological reactions in the cell. Studies over the past century have greatly improved our understanding of the factors that contribute to the catalytic efficiency of enzymes (80, 81). These factors include, among others, the specificity of an enzyme for its substrate, the correct orientation of its reacting groups at the active site relative to the substrate, and its ability to provide electrostatic shielding of charged intermediates in the reaction. In addition, many mechanisms of rate acceleration have been shown to play an important role in catalysis, such as general acid-base catalysis, and covalent catalysis. These mechanisms are, however, not sufficient to rationalize the extraordinary rate enhancement provided by enzymes. Although other mechanisms have been considered in the past 70 years, most have remained in the realm of hypotheses, due, in part, to the difficulty of designing experiments to quantify their importance. One such mechanism is the hypothesis known as strain-induced catalysis. Viewed from the transition state theory of chemical reactions (82, 83), it is well accepted that to catalyze biochemical reactions, enzymes must lower the activation barrier for the substrate to reach the transition state. Due to the intrinsically different structures of the substrate and the transition state, it is almost certain that the enzyme active center cannot be perfectly complementary to both at the same time. In the 1930s, J.B.S. Haldane suggested that enzymes cannot be efficient catalysts if they are fully complementary to the substrate. Rather, he suggested, enzymes must exert strain on the substrate upon binding. He wrote, ". . . the key does not fit the lock perfectly but exercises a certain strain on it" (84). This idea was elaborated by Pauling in 1946. He pointed out that to accelerate the rate of a reaction, enzymes must display complementarity to the transition state. He wrote, "The only reasonable picture of the catalytic activity of enzymes is that which involves an active region of the surface of the enzyme which is closely complementary in structure not to the substrate molecule itself in its normal configuration, but rather to the substrate molecule in a strained configuration, corresponding to the 'activated complex' for the reaction catalyzed by the enzyme" (85). Combined, these two conjectures are known as the Haldane-Pauling hypothesis.

The Haldane-Pauling hypothesis implies the utilization of binding energy to bring about the acceleration of the rate of the reaction, i.e., strain-induced catalysis. To see how the generation of strain could lead to acceleration of the reaction, let us assume that both the enzyme and the substrate are compliant and can deform upon binding. Let the enzyme's active site be complementary not to

the shape of the substrate but to that of the transition state of the reaction. When the substrate first binds, the enzyme is not in a configuration that is catalytically productive. However, because the substrate is not fully complementary to the active site of the enzyme, and the full complement of binding interactions are only realized when the substrate attains the transition state, the enzyme exerts strain on the substrate and this strain favors the attainment of the transition state. It is this gradient of stabilizing binding interactions existing between the substrate and its transition state along the reaction coordinate that amounts to the generation of a force acting on the substrate that ultimately pushes along the reaction. In symbols we can write

$$\frac{\partial E_{bind}}{\partial x_r} = \frac{\partial E_{bind}}{\partial x} \cdot \frac{\partial x}{\partial x_r}, \qquad 25.$$

where E_{bind} is the binding energy gained through complementarity to the enzyme along the reaction coordinate, x_r, and x is the mechanical coordinate through which the substrate is strained. The second factor on the right-hand side expresses the decrease of substrate strain as it moves along the reaction coordinate toward the transition state, whereas the first represents the effective mechanical force exerted by the enzyme on the substrate during this process:

$$F \equiv \frac{\partial E_{bind}}{\partial x}. \qquad 26.$$

These expressions show that whether the enzyme undergoes a conformational change during the process that "drives" the substrate into the transition state or simply provides a gradient of binding interactions along the reaction coordinate that preferentially stabilizes the transition state, the result is the same; in both cases, one can think of the enzyme as exerting a force on the substrate that catalyzes the reaction.

In some cases, the enzyme active site may be more compliant than the substrate and thus, upon binding, the substrate actually induces strain in the enzyme due to its nonideal fit (86). However, such strain will generate an elastic restoring force in the enzyme that will be exerted on the substrate and that, in turn, will tend to distort the substrate to bring about the transition state. In other words, the strain in the enzyme increases the free energy of the enzyme-substrate complex along the reaction coordinate and facilitates the crossing of the transition state beyond which such strain is fully relieved.

The Catalytic Advantage of Transition-State Complementarity

In this model, binding of the substrate to the enzyme induces strain in the complex, and complementarity between the enzyme and substrate is fully realized only at the transition state. We illustrate below the advantage of transition-state complementarity in catalysis.

In Michaelis-Menten kinetics, k_{cat} is a first-order rate constant associated with the rate of decomposition of the enzyme-substrate complex into enzyme and products, whereas k_{cat}/K_M is an apparent second-order rate constant for the generation of products starting from the free enzyme and the free substrate (80), and is a measure of the catalytic efficiency of the enzyme. In symbols,

$$E + S \underset{\Delta G_S}{\overset{K_M}{\longleftrightarrow}} ES \underset{\Delta G^{\ddagger}}{\overset{k_{cat}}{\longrightarrow}} ES^{\ddagger}; \quad E + S \underset{\Delta G_T^{\ddagger}}{\overset{k_{cat}/K_M}{\longrightarrow}} ES^{\ddagger}$$

where ΔG_S is the binding free energy in the association of the enzyme and the substrate, and $\Delta G^{\ddagger}$ and $\Delta G_T{}^{\ddagger}$ are the activation free energies from the ES complex and from the unbound $E + S$, respectively (Figure 7).

The importance of transition-state complementarity is illustrated in Figure 7 under conditions in which $[S] \gg K_M$ and $[S] < K_M$, and when the active site is complementary to the substrate and to the transition state of the reaction (see 80). Here, we assume that the maximum possible free energy of association between enzyme and substrate is $\Delta G_{S,max}$, which arises only when there is full complementarity between enzyme and substrate. If instead, the enzyme is ideally complementary to the transition state $ES^{\ddagger}$, an adverse free energy ΔG_{strain} arising from the strain between the enzyme and substrate contributes to substrate binding: $\Delta G_S = \Delta G_{S,max} + \Delta G_{strain}$. ($\Delta G_S$, $\Delta G_{S,max} < 0$ when $[S] \gg K_M$; and ΔG_S, $\Delta G_{S,max} > 0$ when $[S] < K_M$.) In addition, the free energy of the transition state is lowered by strain. Note that the expressions for the rate of the reaction depend on whether or not the enzyme is saturated with the substrate. However, in both cases, it is catalytically advantageous for the enzyme to be fully complementary to the transition state (thus inducing strain in the substrate) because the effect is to raise both K_M and k_{cat}. Furthermore, transition-state complementarity maximizes the value of k_{cat}/K_M, the catalytic efficiency of the enzyme. This conclusion is valid regardless of whether the enzyme is saturated with the substrate or not.

Although it is difficult to determine the substrate concentrations in vivo, the cases that have been studied, such as those of the glycolytic pathway (87), indicate that enzymes mostly operate under subsaturation conditions (88), i.e.,

Figure 7 Illustration of the advantage of transition state complementarity as discussed in the text. Dashed lines illustrate the free energy when the enzyme binding pocket is complementary to the substrate; solid lines illustrate the free energy for the case of transition state complementarity. Algebraically positive (negative) energies are indicated by arrows pointing upward (downward). (*a*) $[S] \gg K_M$. K_M, k_{cat}, and k_{cat}/K_M are increased by transition state complementarity, and the rate of catalysis increases with k_{cat}. (*b*) $[S] < K_M$. K_M, k_{cat}, and k_{cat}/K_M are increased by transition-state complementarity, and the rate of catalysis increases with k_{cat}/K_M.

a. $[S] >> K_M$

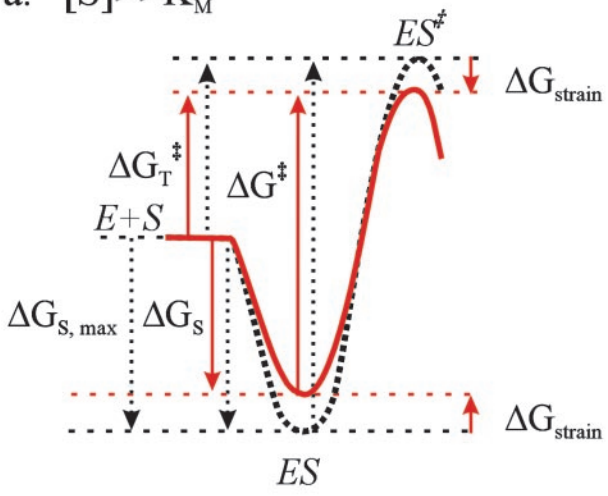

$$v = k_{cat}[E]_0$$

b. $[S] < K_M$

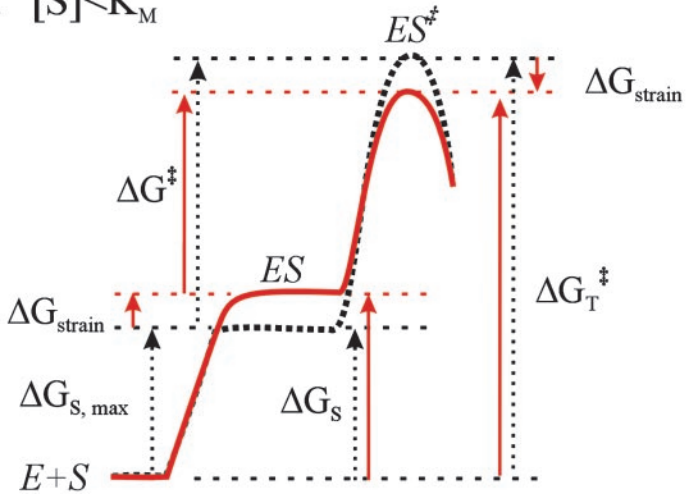

$$v = \frac{k_{cat}}{K_M}[E][S]$$

where substrate concentrations are significantly below their corresponding K_Ms (see Figure 7*b*). Thus, maximum rates of activity can be obtained if these enzymes have evolved to display full complementarity to the transition state such that k_{cat}/K_M is maximized. Furthermore, a high K_M maximizes the concentration of free enzyme [*E*]. These two conditions ensure the maximum efficiency under subsaturating conditions, i.e., $v = k_{cat}/K_M[E][S]$ (80).

Experimental Evidence for Strain-Induced Catalysis

It has been difficult to demonstrate unequivocally the importance of strain in enzyme catalysis. This is in part due to the lack of methods to directly monitor this elusive mechanical property. Even in cases in which enzymes have been cocrystallized with their substrates or with their substrates near or at the transition state, it is difficult to deduce a priori the energies and forces involved in the enzyme/substrate complex.

Structural studies of enzymes with and without their substrates show clear conformational changes of the enzyme and/or its substrate. A well-known example is hexokinase. Hexokinase catalyzes the transfer of a phosphoryl group from ATP to a substrate, such as glucose or mannose. X-ray crystallographic studies of yeast hexokinase showed that the binding of glucose induces a large conformational change in the enzyme (89, 90). Hexokinase comprises two lobes that form a cleft. Upon binding of the glucose, the cleft between the lobes closes, and the bound glucose becomes surrounded by protein. The substrate-induced closing of the cleft in hexokinase provides an excellent example of the induced-fit mechanism (91, 92).

A complementary technique that probes the dynamics of the enzyme-substrate interaction is fluorescence resonance energy transfer (FRET) (93, 94). A recent FRET study of the enzyme EcoRI, a type II restriction endonuclease, resolved large conformational changes in the N terminus, a region essential for tight binding of the DNA. The conformational changes revealed by the FRET experiments are not visible in any of the crystal structures (95).

More experimental evidence for the development of strain during enzyme catalysis has been indirect through the demonstration of two related issues: enzyme complementarity to the transition state, and the utilization of binding energy in catalysis. The former argument dates back to the 1940s when Pauling suggested that complementarity implied that enzymes should bind more strongly to analogs of the transition state than to the free form of their substrates. Pauling's ideas have been confirmed experimentally and further supported by the generation of catalytic antibodies (81, 96, 97).

Yin et al. (98) recently obtained direct physical evidence for substrate strain in antibody catalysis. These authors raised an antibody to a strained mimic of a substrate of the enzyme ferrochelatase. This mimic has a pyrrole nitrogen pushed

out of planarity, a distortion thought to duplicate that involved in the transition state of the reaction (99). Not only does the crystal structure of the antibody complexed with the unstrained substrate show the same distortion, but the antibody also catalyzes its metallation by Zn^{2+} with a catalytic efficiency comparable to that of ferrochelatase. Hokenson et al. (100) studied strain in the carbonyl bond of the substrate of beta-lactamase. Here, a shift in the carbonyl stretch frequency of the beta-lactam substrate upon binding indicated that this bond is stretched in the ES complex; from the frequency shift, the strain in the carbonyl bond can be calculated to be about 3%. Values of the strain of about twice this value have been found in similar systems (101). A final example shows how release of enzyme strain appears to be involved in the catalysis of the reaction by the enzyme-coenzyme complex between aspartate aminotransferase and pyridoxal-5′-phosphate (PLP). Here, crystallographic studies indicated that steric interactions result in the critical hydrogen bond of the protonated Schiff base between the enzyme and PLP being strained in an out-of-plane conformation (102). Because this bond is broken in all ES intermediates and in the transition state, the activation energy to attain the transition state from the unbound E and S is decreased by 16 kJ/mol relative to the unstrained situation, thus decreasing the activation energy of k_{cat}/K_M whose value is increased 10^3-fold. Note that strain in the enzyme, as opposed to the more traditional strain in the substrate, is used in the catalysis by this enzyme.

The Magnitude of the Enzyme-Substrate Forces

The three-dimensional structure of proteins is maintained by a large number of weak interactions and thus, there is a limit to the magnitude of forces and strains that can develop between the enzyme and its substrate in the course of a reaction while maintaining the enzyme's structural integrity. Moreover, the mechanical properties of enzymes, such as their elastic modulus and compressibility, are expected to be anisotropic and inhomogeneous, i.e., to vary with their location within the enzyme and to depend on the direction along which they are measured. Thus, it is difficult to treat this problem in all generality without considering the specific interactions between a particular enzyme and its substrate. Nonetheless, general concepts from the basic physics of deformation can give some insight into the magnitude of the forces and strains that can result from the formation of the ES complex.

It is instructive to consider a simple, elastic, and linear model of the generation of strain in the interaction between enzyme and substrate. Here, we follow the treatment of Gavish (103). Let the complementary surfaces of the enzyme and substrate be depicted as in Figure 8. Here L and l are the length dimensions of the protein and the substrate before binding interactions are turned on, and x and y are the change in these quantities as a result of these interactions. Also, κ_E and κ_S are the spring constants of the enzyme wall and substrate, respectively. Finally,

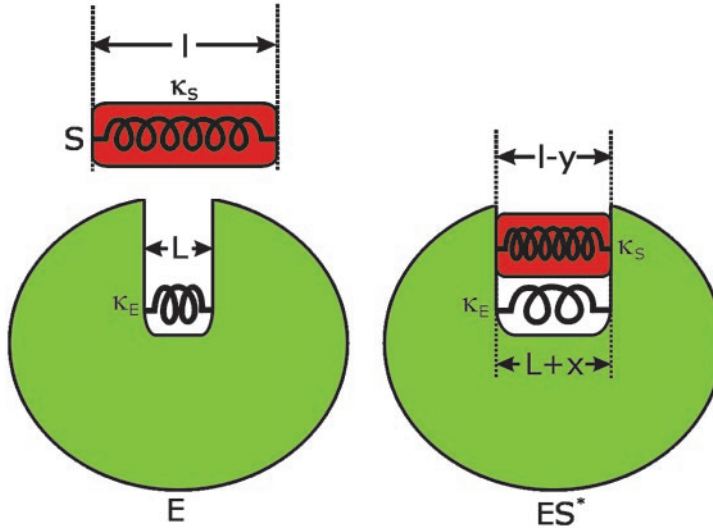

Figure 8 Pictorial representation of the strain induced between the binding pocket of the enzyme and its substrate. (*left*) The enzyme and substrate in their unbound conformations with initial lengths L and l, respectively. (*right*) Distortion is induced upon binding. The enzyme and substrate distort to achieve a net length change (l-L), where the distortion is shared between the enzyme and the substrate according to their relative stiffnesses κ_E and κ_S, as discussed in the text.

F_S and E_{strain} are the force acting on the substrate and the total elastic energy stored in both substrate and enzyme due to the strain. Then it is easy to show that

$$y = \frac{\kappa_E}{\kappa_S + \kappa_E}(l - L), \quad F_S = \frac{\kappa_S \kappa_E}{\kappa_S + \kappa_E}(l - L), \text{ and } E_{strain} = \frac{1}{2}\frac{\kappa_S \kappa_E}{\kappa_S + \kappa_E}(l - L)^2. \quad 27.$$

Note that when $\kappa_E \sim \kappa_S$ the distortion y is half of its maximum possible value (l - L). Under these conditions, the strain and stress on the substrate can be written (103)

$$Strain = \frac{n\Delta A(l - L)}{2V_S}; \quad Stress = -\frac{1}{\beta}\frac{n\Delta A(l - L)}{2V_S} \quad 28.$$

where n is the number of interactions between the substrate and the enzyme, ΔA is the area of interaction in the substrate, β the isothermal compressibility of the protein, and V_S is the volume of the substrate. Using l - $L \sim 2$ Å, $\Delta A \sim 10$ Å^2, $V_S \sim 200$ Å^3 and $\beta \sim 10^{-6}$ atm^{-1}, Gavish obtained values of strain $\sim$ 4%, stress $\sim 2 \times 10^4$ atm, and a stored strain energy of $\sim$1 kcal/mol per interaction. These values correspond to a force of $\sim$50 pN exerted through each interaction

on the substrate. For multiple enzyme-substrate interactions, the stored strain energy becomes considerable, and for four interactions would give rise to a catalytic rate enhancement of $\sim 10^3$.

This simple model and calculation show that several interactions working on the substrate can lead to the development of significant stress and strain in the substrate. Indeed, the enzyme and substrate are engaged through multiple interactions, and it is the sum of all these interactions, each of them weak if compared to a covalent bond, that ultimately determines the degree of strain induced in the substrate. Moreover, an enzyme may distort a substrate by pulling in some locations and pushing in others, thus amplifying the mechanical gain (its mechanical advantage) by using a lever design.

Proteins are likely to be more difficult to compress than to stretch. As discussed above, the maximum force that a protein can support before unfolding in either case will depend on the rate at which the force is applied. As a result, it is possible that larger forces than those calculated above can develop in the formation of ES complexes if the force is the result of compression of the substrate and if it is applied only transiently during the catalytic cycle. Such a scenario may occur when the enzyme possesses a cleft that closes upon substrate binding, as is the case for lysozyme (104–106), for example. In fact, many authors have speculated that one reason why enzymes may have evolved to be so large is to increase their mechanical rigidity (107) and thus to be able to generate larger stresses and strains on substrates by compression.

Enzymes as Mechanical Devices

Here, we pose the following questions: Are enzymes mechanical devices capable of actively exerting force on their substrates through a coordinated set of motions akin to the movements of levers and arms of macroscopic machines? Can enzyme movements direct, guide, and mechanically promote the flux and orientation of chemical groups inside the active site as the reaction proceeds (108)? What would be required for these types of machine-like motions to occur in catalysis?

Enzymes undergo concerted conformational changes upon substrate binding, as postulated by the induced-fit hypothesis (91). In this view of enzyme catalysis, the enzyme, fueled by a sequence of successive binding interactions, undergoes a series of motions to bring a substrate into the transition state and to facilitate and push the catalytic process along its reaction coordinate. Indeed, by studying molecular motors, we have learned a great deal about how a series of concerted mechanical motions can be coupled to energy sources such as the binding and hydrolysis of fuel molecules. Like molecular motors, enzymes should be able to function as mechanical devices undergoing a series of concerted movements by utilizing the potential energy stored in the binding of their substrates or cofactors or in the release of the product of the reaction.

Imagine the binding of a ligand on the surface of a globular protein. Locally, the target region on the macromolecule is formed with the participation of groups

from regions both close and far removed from each other in the sequence. Maintaining the architecture of this region of the surface, as that of any other part of the molecule, requires the appropriate balance of forces and interactions between the groups that form the target binding area and between groups located farther away at some radial distance from this area. To gain insight into the ability of proteins to behave as mechanical devices capable of "pushing along" the reaction, we need to know how efficiently the strain in one part of the molecule transfers to another because this mechanical communication between adjacent regions of the molecule would be needed for the enzyme to carry out a series of concerted conformational changes. Unfortunately, such information is not yet available. Some evidence exists that steric strain occurs predominantly in regions involved with function, presumably because of the more stringent precision needed for ligand binding and catalysis (109). However, much less is known about changes in strain that result from ligand binding, how far the perturbation brought about by this binding propagates into the macromolecule, or the contribution of side groups to the strain in the structure. Direct experimental measurements of mechanical forces have provided much insight into the mechanical stability of proteins and into the mechanisms by which molecular motors can generate force. We anticipate that similar approaches will be used to gain greater insight into the ability of enzymes to release stored substrate-binding energy (in the form of mechanical strain) to catalyze their reactions.

Single-molecule manipulation methods provide the possibility of directly testing some of the main ideas in strain-induced enzymatic catalysis. The mechanics of the enzyme-substrate interaction can be probed by exerting external mechanical force on the enzyme, the substrate, or both. For example, by applying external mechanical force to the two lobes of hexokinase, it should be possible to directly affect either the formation of the ES complex from the free reactants in solution or, possibly, the attainment of the transition state. If the closure of the cleft is rate-limiting, the external force will significantly affect the rate of the reaction, providing direct evidence for the effect of strain in enzyme catalysis. Moreover, by varying the magnitude of the external force applied to the enzyme-substrate complex, it should be possible to estimate the maximum force generated within the complex.

EPILOGUE

One of the main differences between biological macromolecules and their small organic and inorganic counterparts lies in the number, strength, and nature of the interactions that maintain their three-dimensional structures. The large number of relatively weak interactions that stabilize the tertiary structures of macromolecules also confer on these molecules their unique structural adaptability and flexibility in the cell. Often, this structural pliability is manifested in the form of a conformational change that ensues from the binding interactions of macromol-

ecules with other macromolecules or with small ligands. The concept of conformational change that has played a central role in traditional biochemical studies is also essential to the new description proposed in this review: The energy released through binding interactions or bond hydrolysis leads to molecular displacements and to the generation of forces and mechanical work along a coordinate. The significance of this new description resides in the fact that it makes it possible to directly associate energies in the form of mechanical work along a particular coordinate with the corresponding changes in structure. In the next few years the basic mechanical nature of many more essential biochemical processes will likely be recognized and studied in this fashion. We hope that these processes will be amenable to study and characterization by some of the same concepts and experimental methods described in this review.

The *Annual Review of Biochemistry* is online at http://biochem.annualreviews.org

LITERATURE CITED

1. Tinoco I, Bustamante C. 2002. *Biophys. Chem.* 101:513–33
2. Bustamante C, Marko JF, Siggia ED, Smith S. 1994. *Science* 265:1599–600
3. Marko JF, Siggia ED. 1995. *Macromolecules* 28:8759–70
4. Liphardt J, Onoa B, Smith SB, Tinoco I, Bustamante C. 2001. *Science* 292: 733–37
5. Tinoco I. 2004. *Annu. Rev. Biophys. Biomol. Struct.* 33:363–85
6. Bell GI. 1978. *Science* 200:618–27
7. Kramers HA. 1940. *Physica* 7:284–304
8. Eyring H. 1935. *J. Chem. Phys.* 3: 107–15
9. Gautel M, Goulding D. 1996. *FEBS Lett.* 385:11–14
10. Linke WA, Ivemeyer M, Olivieri N, Kolmerer B, Ruegg JC, Labeit S. 1996. *J. Mol. Biol.* 261:62–71
11. Linke WA, Rudy DE, Centner T, Gautel M, Witt C, et al. 1999. *J. Cell Biol.* 146: 631–44
12. Hynes RO. 1990. *Fibronectins*. New York: Springer
13. Shrestha P, Mori M. 1997. *Tenascin: An Extracellular Matrix Protein in Cell Growth, Adhesion and Cancer*. Austin, Texas: Landes Biosci.
14. Krammer A, Lu H, Isralewitz B, Schulten K, Vogel V. 1999. *Proc. Natl. Acad. Sci. USA* 96:1351–56
15. Matouschek A. 2003. *Curr. Opin. Struct. Biol.* 13:98–109
16. Kenniston JA, Baker TA, Fernandez JM, Sauer RT. 2003. *Cell* 114:511–20
17. Saibil HR, Ranson NA. 2002. *Trends Biochem. Sci.* 27:627–32

17a. Valpuesta JM, Martin-Benito J, Gomez-Puertas P, Carrascosa JL, Willison KR. 2002. *FEBS Lett.* 529:11–16

18. Shtilerman M, Lorimer GH, Englander WS. 1999. *Science* 284:822–25
19. Liphardt J, Dumont S, Smith SB, Tinoco I, Bustamante C. 2002. *Science* 296: 1832–35
20. Jarzynski C. 1997. *Phys. Rev. Lett.* 78:2690–93
21. Hummer G, Szabo A. 2001. *Proc. Natl. Acad. Sci. USA* 98:3658–61
22. Evans E, Ritchie K. 1999. *Biophys. J.* 76: 2439–47
23. Oberhauser AF, Hansma PK, Carrion-Vazquez M, Fernandez JM. 2001. *Proc. Natl. Acad. Sci. USA* 98:468–72
24. Friedsam C, Wehle AK, Kuhner F, Gaub HE. 2003. *J. Phys. Condens. Matter* 15: S1709–23

25. Best RB, Fowler SB, Toca-Herrera JL, Clarke J. 2002. *Proc. Natl. Acad. Sci. USA* 99:12143–48
26. Best RB, Brockwell DJ, Toca-Herrera JL, Blake AW, Smith DA, et al. 2003. *Anal. Chim. Acta* 479:87–105
27. Williams PM, Fowler SB, Best RB, Toca-Herrera JL, Scott KA, et al. 2003. *Nature* 422:446–49
28. Evans E. 1998. *Faraday Discuss.* 111: 1–16
29. Fowler SB, Best RB, Herrera JLT, Rutherford TJ, Steward A, et al. 2002. *J. Mol. Biol.* 322:841–49
30. Paci E, Karplus M. 2000. *Proc. Natl. Acad. Sci. USA* 97:6521–26
31. Tinoco I, Bustamante C. 1999. *J. Mol. Biol.* 293:271–81
32. Onoa B, Dumont S, Liphardt J, Smith SB, Tinoco I, Bustamante C. 2003. *Science* 299:1892–95
33. Marszalek PE, Lu H, Li HB, Carrion-Vazquez M, Oberhauser AF, et al. 1999. *Nature* 402:100–3
34. Lenne P-F, Raae AJ, Altmann SM, Saraste M, Horber JKH. 2000. *FEBS Lett.* 476:124–28
35. Oberhauser AF, Badilla-Fernandez C, Carrion-Vazquez M, Fernandez JM. 2002. *J. Mol. Biol.* 319:433–47
36. Li H, Linke WA, Oberhauser AF, Carrion-Vazquez M, Kerkvliet JG, et al. 2002. *Nature* 418:998–1002
37. Rief M, Pascual J, Saraste M, Gaub HE. 1999. *J. Mol. Biol.* 286:553–61
38. Carrion-Vazquez M, Li H, Lu H, Marszalek PE, Oberhauser AF, Fernandez JM. 2003. *Nat. Struct. Biol.* 10: 738–43
39. Brockwell DJ, Paci E, Zinober RC, Beddard GS, Olmsted PD, et al. 2003. *Nat. Struct. Biol.* 10:731–37
40. Lu H, Schulten K. 1999. *Proteins: Struct. Funct. Genet.* 35:453–63
41. Li HB, Carrion-Vazquez M, Oberhauser AF, Marszalek PE, Fernandez JM. 2000. *Nat. Struct. Biol.* 7:1117–20
42. Carrion-Vazquez M, Oberhauser AF, Fisher TE, Marszalek PE, Li HB, Fernandez JM. 2000. *Prog. Biophys. Mol. Biol.* 74:63–91
43. Matouschek A, Bustamante C. 2003. *Nat. Struct. Biol.* 10:674–76
44. Kellermayer MSZ, Smith SB, Granzier HL, Bustamante C. 1997. *Science* 276: 1112–16
45. Kellermayer MSZ, Smith SB, Bustamante C, Granzier HL. 2001. *Biophys. J.* 80:852–63
46. Li HB, Oberhauser AF, Fowler SB, Clarke J, Fernandez JM. 2000. *Proc. Natl. Acad. Sci. USA* 97:6527–31
47. Law R, Carl P, Harper S, Dalhaimer P, Speicher DW, Discher DE. 2003. *Biophys. J.* 84:533–44
48. Wang MD, Schnitzer MJ, Yin H, Landick R, Gelles J, Block SM. 1998. *Science* 282:902–7
49. Wuite GJL, Smith SB, Young M, Keller D, Bustamante C. 2000. *Nature* 404: 103–6
50. Delagoutte E, von Hippel PH. 2003. *Q. Rev. Biophys.* 36:1–69
51. Delagoutte E, von Hippel PH. 2002. *Q. Rev. Biophys.* 35:431–78
52. Strick TR, Croquette V, Bensimon D. 2000. *Nature* 404:901–4
53. Dekker NH, Rybenkov VV, Duguet M, Crisona NJ, Cozzarelli NR, et al. 2002. *Proc. Natl. Acad. Sci. USA* 99:12126–31
54. Stone MD, Bryant Z, Crisona NJ, Smith SB, Vologodskii A, et al. 2003. *Proc. Natl. Acad. Sci. USA* 100:8654–59
55. Smith DE, Tans SJ, Smith SB, Grimes S, Anderson DL, Bustamante C. 2001. *Nature* 413:748–52
56. Boyer PD. 2001. *Biochemistry* 66: 1058–66
57. Berg HC. 2003. *Annu. Rev. Biochem.* 72: 19–54
58. Hua W, Young EC, Fleming ML, Gelles J. 1997. *Nature* 388:390–93
59. Schnitzer MJ, Block SM. 1997. *Nature* 388:386–90
60. Davenport RJ, Wuite GJL, Landick R,

Bustamante C. 2000. *Science* 287: 2497–500
61. Keller D, Bustamante C. 2000. *Biophys. J.* 78:541–56
62. Coppin CM, Pierce DW, Hsu L, Vale RD. 1997. *Proc. Natl. Acad. Sci. USA* 94:8539–44
63. Visscher K, Schnitzer MJ, Block SM. 1999. *Nature* 400:184–89
64. Yin H, Wang MD, Svoboda K, Landick R, Block SM, Gelles J. 1995. *Science* 270: 1653–57
65. Oster G, Wang H. 2003. In *Molecular Motors*, ed. M. Schliwa, pp. 207–27. Weinheim: Wiley-VCH Verlag GmbH
65a. Itoh H, Takahashi A, Adachi K, Noji H, Yasuda R, et al. 2004. *Nature* 427: 465–68
66. Finer JT, Simmons RM, Spudich JA. 1994. *Nature* 368:113–19
67. Molloy JE, Burns JE, Kendrickjones J, Tregear RT, White DCS. 1995. *Nature* 378:209–12
68. Svoboda K, Schmidt CF, Schnapp BJ, Block SM. 1993. *Nature* 365:721–27
69. Nishiyama M, Muto E, Inoue Y, Yanagida T, Higuchi H. 2001. *Nat. Cell Biol.* 3:425–28
70. Yasuda R, Noji H, Kinosita K, Yoshida M. 1998. *Cell* 93:1117–24
71. Adachi K, Noji H, Kinosita K. 2003. *Methods Enzymol.* (Pt. B) 361:211–27
72. Guo P, Peterson C, Anderson D. 1987. *J.Mol. Biol.* 197:229–36
73. Block SM, Asbury CL, Shaevitz JW, Lang MJ. 2003. *Proc. Natl. Acad. Sci. USA* 100:2351–56
74. Wang HY, Elston T, Mogilner A, Oster G. 1998. *Biophys. J.* 74:1186–202
75. Thomen P, Lopez PJ, Heslot F. 2004. Submitted
76. Uemura S, Ishiwata S. 2003. *Nat. Struct. Biol.* 10:308–11
77. Uemura S, Kawaguchi K, Yajima J, Edamatsu M, Toyoshima YY, Ishiwata S. 2002. *Proc. Natl. Acad. Sci. USA* 99: 5977–81
78. Dimroth P, Wang HY, Grabe M, Oster G. 1999. *Proc. Natl. Acad. Sci. USA* 96: 4924–29
79. Oster G, Wang H, Grabe M. 2000. *Philos. Trans. R. Soc. London Ser. B* 355: 523–28
80. Fersht A. 1985. *Enzyme Structure and Mechanism*. New York: Freeman.
81. Jencks WP. 1987. *Catalysis in Chemistry and Enzymology*. New York: Dover.
82. Eyring H. 1935. *Chem. Rev.* 17:65–77
83. Pelzer H, Wigner E. 1932. *Z. Phys. Chem. B* 15:445
84. Haldane JBS. 1965. *Enzymes*. Cambridge: M.I.T. Press.
85. Pauling L. 1946. *Chem. Eng. News* 24: 1375–77
86. Bernstein BE, Michels PA, Hol WG. 1997. *Nature* 385:275–78
87. Lowry OH, Passonneau JV. 1964. *J. Biol. Chem.* 239:31–42
88. Atkinson DE. 1969. In *Current Topics in Cellular Regulation*, ed. ER Stadtman, BL Horecker, pp. 29–43. New York: Academic
89. Bennett WS Jr, Steitz TA. 1978. *Proc. Natl. Acad. Sci. USA* 75:4848–52
90. Bennett WS Jr, Steitz TA. 1980. *J. Mol. Biol.* 140:211–30
91. Koshland DE. 1958. *Proc. Natl. Acad. Sci. USA* 44:98–104
92. Koshland DE. 1963. *Cold Spring Harbor Symp. Quant. Biol.* 28:473–82
93. Selvin PR. 2000. *Nat. Struct. Biol.* 7: 730–34
94. Selvin PR. 1995. *Methods Enzymol.* 246: 300–34
95. Watrob H, Liu W, Chen Y, Bartlett SG, Jen-Jacobson L, Barkley MD. 2001. *Biochemistry* 40:683–92
96. Tramontano A, Janda KD, Lerner RA. 1986. *Science* 234:1566–70
97. Pollack SJ, Jacobs JW, Schultz PG. 1986. *Science* 234:1570–73
98. Yin J, Andryski SE, Beuscher AE, Stevens RC, Schultz PG. 2003. *Proc. Natl. Acad. Sci. USA* 100:856–61
99. McLaughlin GM. 1974. *J. Chem. Soc.Perkin Trans. 2*:136–40

100. Hokenson MJ, Cope GA, Lewis ER, Oberg KA, Fink AL. 2000. *Biochemistry* 39:6538–45
101. Chittock RS, Ward S, Wilkinson AS, Caspers P, Mensch B, et al. 1999. *Biochem J.* 338 (Pt. 1):153–59
102. Rhee S, Silva MM, Hyde CC, Rogers PH, Metzler CM, et al. 1997. *J. Biol. Chem.* 272:17293–302
103. Gavish B. 1986. In *The Fluctuating Enzyme*, ed. GR Welch, pp. 263–339. New York: Wiley
104. Kelly JA, Sielecki AR, Sykes BD, James MN, Phillips DC. 1979. *Nature* 282: 875–78
105. Blake CC, Johnson LN, Mair GA, North AC, Phillips DC, Sarma VR. 1967. *Proc. R. Soc. London Ser. B* 167:378–88
106. Blake CC, Koenig DF, Mair GA, North AC, Phillips DC, Sarma VR. 1965. *Nature* 206:757–61
107. Narlikar GJ, Herschlag D. 1997. *Annu. Rev. Biochem.* 66:19–59
108. Williams RJP. 1993. *Trends Biochem. Sci.* 18:115–17
109. Herzberg O, Moult J. 1991. *Proteins* 11: 223–29
110. Essevaz-Roulet B, Bockelmann U, Heslot F. 1997. *Proc. Natl. Acad. Sci. USA* 94:11935–40
111. Rief M, Clausen-Schaumann H, Gaub HE. 1999. *Nat. Struct. Biol.* 6:346–49
112. Carrion-Vazquez M, Oberhauser AF, Fowler SB, Marszalek PE, Broedel SE, et al. 1999. *Proc. Natl. Acad. Sci. USA* 96:3694–99
113. Pantazatos DP, MacDonald RI. 1997. *J. Biol. Chem.* 272:21052–59
114. Khorasanizadeh S, Peters ID, Butt TR, Roder H. 1993. *Biochemistry* 32: 7054–63
115. Noji H, Yasuda R, Yoshida M, Kinosita K. 1997. *Nature* 386:299–302
116. Cooke R, Franks K, Luciani G, Pate E. 1988. *J. Physiol.* 395:77–97
117. Mehta AD, Finer JT, Spudich JA. 1997. *Proc. Natl. Acad. Sci. USA* 94:7927–31
118. Veigel C, Bartoo ML, White DCS, Sparrow JC, Molloy JE. 1998. *Biophys. J.* 75: 1424–38
119. Svoboda K, Block SM. 1994. *Cell* 77: 773–84
120. Kojima H, Muto E, Higuchi H, Yanagida T. 1997. *Biophys. J.* 73:2012–22
121. Wang H, Oster G. 2002. *Europhys. Lett.* 57:134–40

Annual Review of Biochemistry
Volume 73, 2004

CONTENTS